3-2023

A Method for Monte Carlo Neutral Particle Radiation Transport in a Variable Density Atmosphere

Aidan B. Edens

A METHOD FOR MONTE CARLO NEUTRAL PARTICLE RADIATION TRANSPORT IN A VARIABLE DENSITY ATMOSPHERE

THESIS

Aidan B Edens

AFIT-ENP-MS-23-M-082

DEPARTMENT OF THE AIR FORCE
AIR UNIVERSITY

AIR FORCE INSTITUTE OF TECHNOLOGY

Wright-Patterson Air Force Base, Ohio

AFIT-ENP-MS-23-M-082

A METHOD FOR MONTE CARLO NEUTRAL PARTICLE RADIATION TRANSPORT IN A VARIABLE DENSITY ATMOSPHERE

THESIS

Presented to the Faculty

Department of Engineering Physics

Graduate School of Engineering and Management

Air Force Institute of Technology

Air University

Air Education and Training Command

in Partial Fulfillment of the Requirements for the

Degree of Master of Science in Nuclear Engineering

Aidan B Edens, B.S.

23 March, 2023

AFIT-ENP-MS-23-M-082

A METHOD FOR MONTE CARLO NEUTRAL PARTICLE RADIATION TRANSPORT IN A VARIABLE DENSITY ATMOSPHERE

THESIS

Aidan B Edens, B.S.

Committee Membership:

Whitman T Dailey, Ph.D
Chair

Jerawan C Armstrong, Ph.D
Member

Darren E Holland, Ph.D
Member

Karen C Kelley, Ph.D
Member

Abstract

The transport of radiation in the atmosphere is important to the study of the effects of nuclear weapons. Quantifying the effects of prompt radiation following a nuclear explosion depends on accurate simulation of the surrounding transport medium. The variable nature of the atmosphere presents a challenge in this regard. This work implements a well-known technique, Mass Integral Scaling (MIS), to perform Monte Carlo radiation transport calculations in a variable density atmosphere. Expanding upon previous implementations where only free-field estimates were possible, the ability to perform transport calculations with other media present – such as clouds – is added. Previous implementations of a variable density atmosphere were shown to be incomplete. This work has improved upon those previous implementations and results studying neutron and photon fluence have been verified against the standard version of Monte Carlo N-Particle Transport Code (MCNP). The result of this work has also shown improvement in simulation run times and in required model complexity.

Acknowledgements

I would like to express my deepest gratitude to my advisor Dr. Whitman Dailey for his exceptional guidance and unwavering support throughout this journey. His patience, expertise, and commitment to my success have been invaluable. I am also grateful to the rest of my committee members for their insightful feedback and constructive criticism, which have helped shape my research and improve its quality. I could not have completed this thesis without their guidance and encouragement, and I am forever grateful for their contributions. Finally, I would like to thank my family for the unyielding support and encouragement they have provided.

Aidan B Edens

Table of Contents

Page

List of Figures

Figure Page

List of Tables

A METHOD FOR MONTE CARLO NEUTRAL PARTICLE RADIATION TRANSPORT IN A VARIABLE DENSITY ATMOSPHERE

I. Introduction

The atmospheric radiation transport problem, specifically the simulation of the prompt radiation following a nuclear explosion, is a complex and multifaceted challenge that requires precise modeling of the variation in density in the atmosphere. A basic approach to modeling radiation transport in variable density media involves the use of discrete regions of constant density to approximate the variation in density. This can lead to errors in the simulation results, as the Monte Carlo method, within the context of radiation transport simulations, assumes a constant density medium for the sampling of the distance to collision for neutral particles such as neutrons and photons. With respect to both accuracy and computational cost, the implementation of a varying density atmosphere in a Monte Carlo radiation transport code would be an improvement in the modeling and simulation of the the atmospheric transport problem.

Furthermore, the ability to accurately represent the influence of density variations on the transport of radiation is a key concern with traditional methods. In a constantly varying density atmosphere, the probability of collision and the distance traveled by a particle before a collision can vary substantially. It is important to recognize that the variable density is just one aspect of a larger problem. Other factors may need consideration depending on the problem scope such as the earth's curvature, weather, and gravity, though these are just a few examples. Accurate predictions of the effects of prompt radiation are important for the assessment of nuclear

weapons effects.

When solutions to the atmospheric radiation transport problem were first sought, techniques other than the computationally expensive Monte Carlo method were pursued. One approach to the problem, Mass Integral Scaling (MIS), was adopted early on and implemented in computer codes such as SMAUG [1] and ATR [2]. The SMAUG code used empirical functions fit to data from a discrete ordinates code, providing faster and simpler calculations compared to the Monte Carlo method.

With an earlier version of the Monte Carlo N-Particle Transport Code (MCNP) produced by Los Alamos National Laboratory (LANL), Monti [3] integrated the MIS approach with the Monte Carlo method. In a comparison of the MIS implementation within the modified MCNP and the SMAUG code, the SMAUG code overestimated the neutron fluence at longer mass ranges [4]. Almost twenty years after Monti's modification, Mashnik [5] re-implemented the method with a more recent version of MCNP (Version 6) and successfully replicated Monti's results. Most notably, one of Mashnik's tests reported improved runtimes compared to the unmodified version of MCNP6. Although this was a notable improvement to the atmospheric radiation transport problem, MIS is still an approximation to the problem as it assumes a flat-earth i.e. the change in density is strictly a function of altitude.

A more recent method for solving the atmospheric radiation transport problem is the effective path length (EPL) proposed by Dailey [6]. This method was demonstrated in the Air Force Institute of Technology's High-Altitude to Space Transport Estimator (HASTE) [7] code and, whereas MIS method assumes a flat-earth, the EPL method can account for other geometries including a spherical or arbitrary Earth shape model. This feature is especially relevant when considering both problems where the source and detector are near co-altitude and far apart; with MIS, the density remains constant but with EPL the density changes throughout the straight-line

path.

With typical Monte Carlo radiation transport codes, users are required to model the atmosphere with many discrete homogeneous layers. For calculations covering long distances, this method leads to increased input complexity, long run-times, and the potential for low-fidelity results. The goal of this work is to create and verify a feature within MCNP for the atmospheric radiation transport community. To address the issues of input complexity, run-times, and confidence in results, two separate approaches will be investigated: the MIS approach and the sub-stepping approach. Both approaches will incorporate a variable density atmosphere model based on the U.S. Standard Atmosphere, 1976 (USSA) [8]. In contrast to previous works that were limited to free field calculations, this project broadens the scope of calculations to include problems where other media are present and must be considered in the analysis.

II. Background & Theory

2.1 Preamble

The CRAY-1 supercomputer was introduced in 1976 and had a clock speed of 80 MHz. It was capable of performing approximately 160 million FLOPs (floating point operations per second). In comparison, the average laptop today has a clock speed of around 2-3 GHz and is capable of performing hundreds of billions of FLOPs. This means that the average laptop today is approximately one million times more powerful than the CRAY-1. As a result, the atmospheric radiation transport problem is more approachable now than it was in the past. This chapter details the relevant background and theory for this work. First, the relevant features of the atmosphere and a representative model are discussed. The Monte Carlo method is then introduced along with a description of the MCNP code. Finally, different methods of performing radiation transport simulations in varying media are covered.

2.2 The Atmosphere

There are two features of the atmosphere relevant to this work: the isotope composition and the density. Both of these features vary with altitude. In general, the density of air trends with increasing altitude as a decaying exponential shown in Figure 1. This trend, however, is not representative of a singular exponential function.

2.2.1 U.S. Standard Atmosphere, 1976

The U.S. Standard Atmosphere, 1976 (USSA) [8] is a model of the Earth's atmosphere that is used to standardize atmospheric measurements and calculations. The model makes several assumptions about the atmosphere, including that it is dry and it is turbulently mixed below an altitude of 86 kilometers. The USSA is based on an

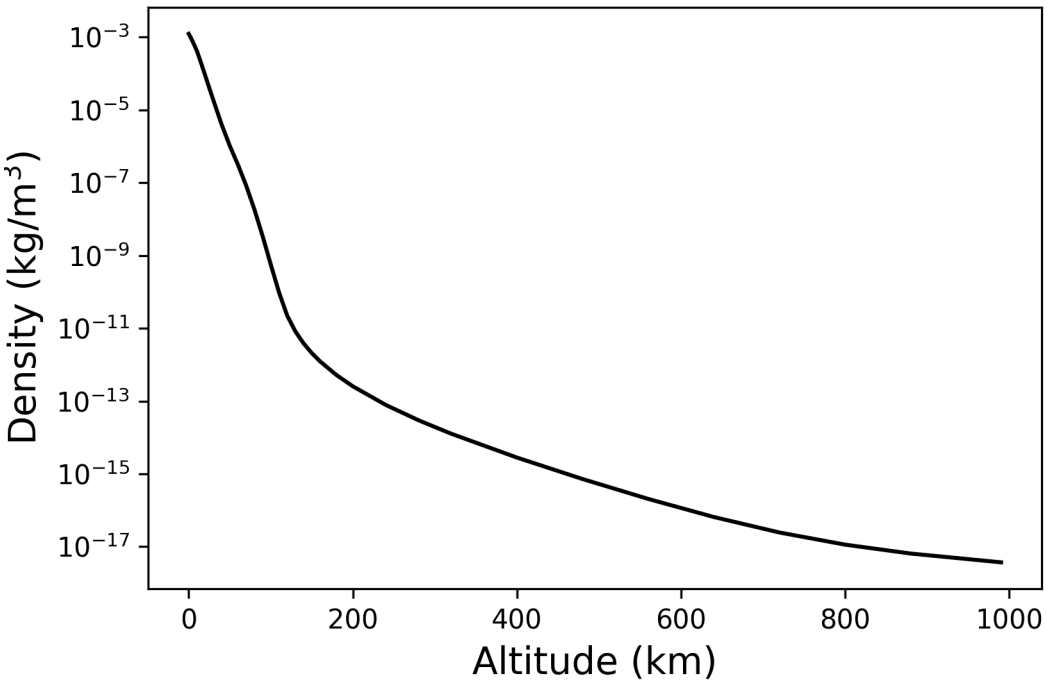

Figure 1: Air density vs. geometric altitude from U.S. Standard Atmosphere Tables, 1976 [8]

average location of 45 degrees latitude and 60 degrees longitude, and is applicable to the United States and surrounding regions. The assumption of a turbulently mixed atmosphere below 86 kilometers translates to a constant fractional composition of gas species defined in Table 2.2.1. Beyond 86 kilometers, the diffusion of individual gas species begins to take significant effect and hydrostatic equilibrium breaks down [8].

Rather than directly calculate the density of the atmosphere, the trend may be approximated with a set of continuous piece-wise exponential functions. Separated into regions by altitude, the air density at any geometric altitude is given analytically by:

$$\rho(Z) = \rho(Z_i) \exp\left[-\frac{Z - Z_i}{S_i}\right], \tag{1}$$

Table 1: Assumed fractional composition of sea-level dry air

Gas Species	Fractional Volume
N_2	0.78084
O_2	0.209476
Ar	0.00934
CO_2	0.000314
Ne	0.00001818
He	0.00000524
Kr	0.00000114
Xe	0.000000087
CH_4	0.000002
H_2	0.0000005

where $\rho(Z)$ is the density at a specified altitude Z, $\rho(Z_i)$ is the density at the base altitude of the ith region, and S_i is the density scale height factor of the ith region. This expression was developed for Monti's application of a variable density atmosphere in MCNP and received further use in Mashnik's application [4] [5]. Concerned with the change in mixing ratio between nitrogen and oxygen beyond 86 km, Mashnik performed simulations accounting for this change and reported no appreciable difference between a constant ratio of nitrogen to oxygen at all altitude regimes.

2.3 The Monte Carlo Method

The Monte Carlo method is a statistical method used to simulate and analyze complex systems by randomly sampling the possible outcomes of a process. It is a powerful tool for solving problems in a wide range of fields, including physics, engineering, finance, and computer science. In the context of radiation transport, the Monte Carlo method is used to simulate the interactions of neutral particles with matter. In the analog sense, this is achieved by simulating the sequential probabilistic events that make up a particle's journey, known as its history, from beginning to end. This sequence of events is also referred to as the random walk process. The simulation

of multiple particle histories can be run in parallel, with the probability distributions governing each event being randomly selected to represent the average phenomenon [9].

For neutrons and photons, the fundamental process behind the Monte Carlo method is sampling of the distance to next collision of the particle. In a medium with fixed composition, the probability of collision for a particle between ℓ and $\ell + d\ell$ is given by,

$$\pi(\ell)\, d\ell = \exp(-\Sigma_t \ell) \cdot \Sigma_t d\ell, \tag{2}$$

where Σ_t is the macroscopic cross section and is representative of the probability per unit length of a collision [10]. The probability density function (PDF) of Equation 2 is provided in Equation 3,

$$\pi(\ell) = \Sigma_t \cdot \exp(-\Sigma_t \ell). \tag{3}$$

The associated cumulative distribution function (CDF) follows as

$$\Pi(\ell) = 1 - \exp(-\Sigma_t \ell) = \zeta, \tag{4}$$

where ζ is a random variable sampled on the unit interval $(0, 1]$. Inversion of the CDF yields the following

$$\ell = -\frac{\ln(1-\zeta)}{\Sigma_t} = -\frac{\ln(1-\zeta)}{\sigma_t \rho}, \tag{5}$$

where ℓ is the distance to collision. The macroscopic cross section is illustrated here as the product of the microscopic cross section, σ_t, and density, ρ, of the transport medium. It is evident that the introduction of a medium with either varying density or microscopic cross section introduces complexity in the expression for the distance

to collision. In the case of a varying macroscopic cross section, the CDF becomes Equation 6.

$$\zeta = \int_0^s \Sigma_t(\ell) \cdot \exp\left[-\int_{\ell_0}^{\ell} \Sigma_t(\ell')d\ell'\right] d\ell \tag{6}$$

2.3.1 MCNP

Radiation transport codes such as OpenMC or the Monte Carlo N-Particle Transport Code (MCNP) code developed by Los Alamos National Laboratory (LANL) use constructive solid geometries (CSGs) to create models of the transport system. In MCNP, CSGs are used to define cells which require discrete density values i.e. each cell is assigned a constant density. This presents a challenge for variable density media. Depending on the problem, partitioning the medium into many constant density cells to approximate the change in density may work well. However, this method may lead to increased input complexity, long run-times, and the potential for low-fidelity results due to the increased number of surfaces. Alongside CSGs, a more recent method for modeling geometries with complex surfaces in MCNP involves unstructured mesh (UM). A recent verification and validation study performed by Jeroutek investigated the use of UM to simulate local density variations in deformed geometries [11]. While the use of an UM does not eliminate the use of constant density cells, it may be a useful approach to simulating radiation transport in variable density media.

To run particle transport simulations, users of MCNP provide an input file containing information specific to their problem such as: the geometry specification, the description of materials, the location and characteristics of the particle source, the type of answers desired (tallies), and any non-analog techniques they wish to employ [10]. This information is written in sections of the input file referred to as the cell, surface, and data cards. The general process of MCNP at runtime begins with ini-

tiation (IMCN). At initiation the input file provided by the user is read-in and the problem geometry, particle source, and tallies to be used are processed. Following this, cross section processing (XACT) occurs. With the problem and cross section data known, the main procedure MCRUN handles particle histories. The history for transport of a neutron or photon follows the following procedure [9]

- Start a source particle
- Compute a distance to nearest boundary and sample a distance to next collision
- If the distance to nearest boundary is less than the sampled distance to next collision, the particle cross the boundary and enter as new cell. Otherwise a physics event at the sampled collision point is randomly sampled using nuclear data
- Find the total neutron cross section and process neutron collisions producing photons as appropriate
- Find the total photon cross section and process photon collision producing electrons as appropriate
- Use the optional thick-target bremsstrahlung approximation if no electron transport
- Process detector tallies if requested
- Process surface, cell, and pulse height tallies if requested

2.3.2 Point & Ring Detectors

When calculating a flux-related quantity at a specific point in space in an analog Monte Carlo simulation, the chance of a particle actually reaching that exact point

is small and may require the use of a point detector. This is especially true for optically thick problems. Point detectors are a deterministic method known as a next-event estimator. At each collision along a particle's simulated random walk, a low-weight pseudoparticle is created and directed toward the detector [9]. These particles experience no further collisions on their way to the detector. This allows for the accumulation of many low-weight pseudoparticles at the detector, which is the focus of the calculation, even though no actual particle history would be able to reach the detector [9].

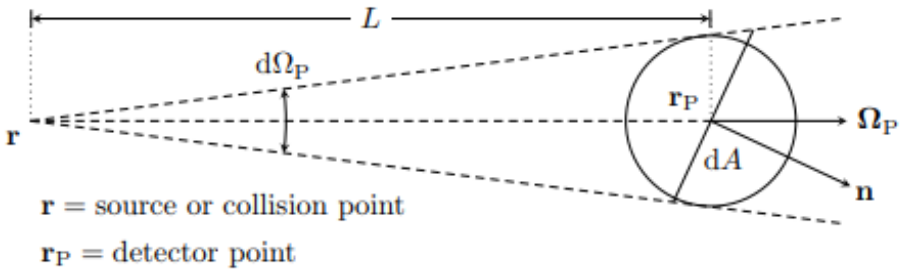

Figure 2: Illustration of point detector contributions [9]

Within MCNP, the point detector (Tally F5) estimate is determined by

$$F5 = w\frac{p\left(\mu\right)}{2\pi L^2}\exp\left[-\int_0^L -\Sigma_t\left(s\right)ds\right], \tag{7}$$

where w is the particle weight, the exponential term accounts for the attenuation between the source and detector, $p(\mu)$ accounts for the probability of scattering toward the detector [10]. The F5 tally requires the selection of a fictitious sphere with radius R_0 centered about the detector point. This is necessary to avoid the potential unbounded variance as L (shown in Figure 2) approaches zero. In other words, if a source or collision event happens in close proximity to the detector, L approaches zero and the flux increases infinitely [9]. In practice, the F5 tally is calculated in two ways. The first way is for cases where L is greater than R_0 i.e. the source or collision

event is not close to the detector. In this case, the contribution to the detector is calculated by

$$F5 = w \cdot p\,(\mu)\, e^{-\tau}. \tag{8}$$

where τ is the optical thickness of the path L. The other way the F5 tally is calculated is for cases where the source or collision event occurs within the fictitious sphere. In this case, the contribution to the detector is calculated with

$$F5 = w \frac{p\,(\mu)}{\frac{2}{3}\pi R_0^3} \left[1 - e^{\Sigma_t \cdot R_0}\right], \tag{9}$$

The F5 tally distinguishes between the total and direct contributions to the detector. The direct, or uncollided, flux refers to the portion of the total flux originating from pseudoparticles at source events. For problems that possess rotational symmetry, which is the case for the atmosphere model employed here, the point detector may be represented instead as a ring to improve the efficiency of the calculation [9]. The improvement in efficiency is a result of biasing the selection of point detector locations to favor those near the contributing source (or collision) point [10]. Because of the optical thickness and spherical divergence experienced by particles, the use of ring detectors is critical for this work.

2.4 Approaches to Radiation Transport in Varying Media

There are many different approaches to radiation transport in media with varying material properties, some of which have a long history of application in Monte Carlo radiation transport. Such methods include sub-stepping, delta-tracking, 'direct method', mass integral scaling, and effective path length.

2.4.1 Sub-stepping

Simulating the transport of neutral particles in a medium with varying material properties may be accomplished with the sub-stepping approach. This approach breaks down the medium into multiple segments. Within each segment, the material density and nuclear cross sections are assumed to be constant. Consider an infinite one-dimensional slab where the microscopic cross section remains constant but the density of the medium increases linearly along $\hat{x}$. The sub-stepping technique may be applied by dividing the slab into many regions and assigning a single density representative of the average density across each individual region, shown in Figure 3.

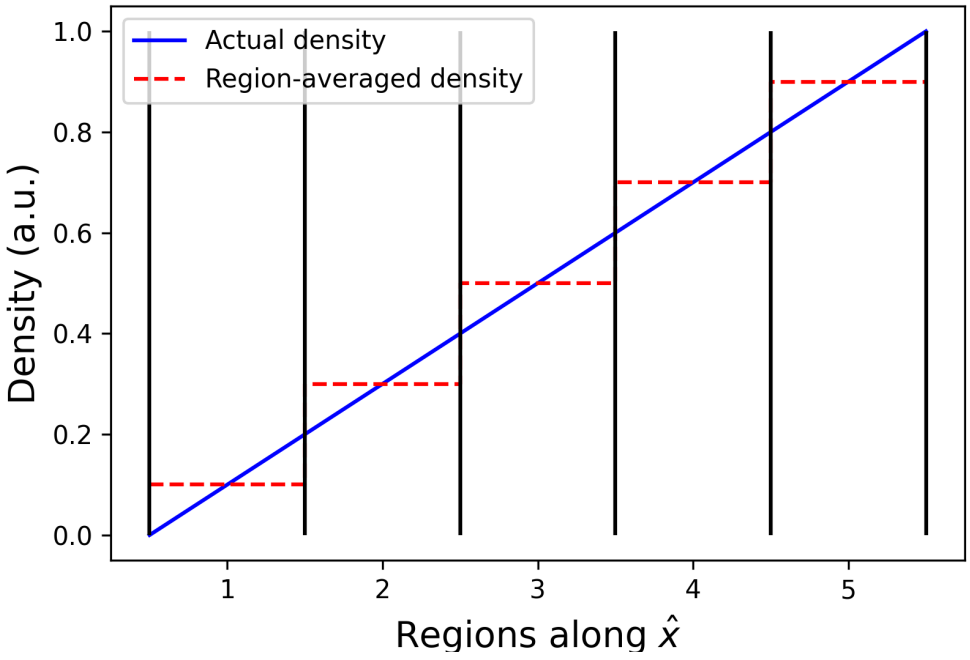

Figure 3: Toy example of the sub-stepping technique.

A particle's behavior can then be modeled traditionally in each segment to determine its behavior along the entire flight path. Depending on the degree of variation

in a medium's density, many layers may be required. As a result, the sub-stepping approach may become computationally intensive due to an increasing number of calculations at boundaries. In addition, this approach requires careful consideration of both the region length and number of regions used in the simulation. For these reasons, sub-stepping is not well suited for simulating the transport of radiation in the atmosphere.

2.4.2 Delta-Tracking

Delta-tracking is a Monte Carlo technique in radiation transport that involves the use of a fictitious or majorant cross section, Σ_{max}, chosen or estimated to be the maximum value expected during the particle's flight. The method involves sampling a trial flight distance using this maximum cross section, moving the particle that distance, and then determining the probability of the flight distance being accepted. If the flight distance is accepted, it is moved again; if it is rejected, the entire procedure is repeated. Relative to the sub-stepping approach, the delta-tracking method has been shown to reduce computation time by eliminating boundaries, and calculations at boundary crossings, in the random-walk procedure [12]. Some drawbacks of this method, however, are its inability to be a track-length estimator and cases where Σ_{max} is much greater than the typical cross section leading to inefficient rejection sampling [13].

Recent works have employed different variants of the original delta-tracking method presented by Woodcock. Such variants include the combination of delta-tracking with ray tracing. This variant improves upon the original method by preferentially switching between delta-tracking and ray tracing in regions where the probability of a real collision is low [12]. The weighted delta-tracking (WDT) technique is another variant of the original method [14]. This method also uses the fictitious cross section to

sample the length of the particle path in a similar way to the original delta-tracking. However, unlike the delta-tracking method, WDT treats all collisions as actual events. In order to account for the virtual collisions that are no longer explicitly taking place, the weight of the particle is adjusted. This is necessary to maintain fairness in the simulation [12].

As with sub-stepping, the delta-tracking method is not ideal for application to the atmospheric transport problem. It is evident from the exponential variation of density shown in Figure 1, the majorant cross section will be much greater than the typical cross section and inefficient rejection sampling will occur. This could be mediated by separating the atmosphere into layers similar to sub-stepping; where each layer has its own majorant cross section. However, this introduces the same considerations and concerns as the sub-stepping method.

2.4.3 Direct Method

Another Monte Carlo technique is the 'direct method' developed by Brown and Martin [15]. This method was investigated for sampling the free-flight distance in the case of varying cross sections and involves randomly sampling the particle's path and then using numerical integration via Newton iteration to solve the resulting set of equations. In their work, Brown and Martin compared the transmission of particles, with scattering ignored, between the direct, delta-tracking, and sub-stepping methods for different profiles of cross-section variation. Some of the profiles considered were constant, linearly increasing, linearly decreasing, and exponentially decreasing. The comparison of the exponentially decreasing profile is of particular interest as it best aligns with the relevant feature of the atmosphere. In their results, values for transmission of particles were reported as 0.7177, 0.7168, and 0.7171 for the sub-stepping, delta-tracking, and direct methods, respectively [15]. This is a promising result, how-

ever, further study is required to quantify the direct methods efficiency relative to the other techniques.

2.4.4 Mass Scaling Law

The mass scaling law can be stated as follows: "**In an infinite homogeneous medium with an isotropic point source, the time-integrated $4\pi R^2$ fluence or dose is only a function of ρR, the mass per unit area between source and receiver** [16]." When the density of the transport medium is constant, the mass range is calculated as the product of the density and slant range between the source and detector, as is the case for constant density air. The mass scaling law, which was initially derived from the Boltzmann transport equation in 1956 by Zerby [17], can also be derived from the diffusion equation, as demonstrated by Shulstad [16], using the same assumptions as Zerby.

As an example of the mass scaling law, consider an isotropic point source placed in two infinite homogeneous media – medium A and medium B. The two media are related by

$$\rho_A R_A = \rho_B R_B, \tag{10}$$

where ρ and R are the density and slant range between source and detector of each respective medium. The energy dependent fluence at each slant range R is given as

$$4\pi R_A^2 F(R_A, E) = 4\pi R_B^2 F(R_B, E), \tag{11}$$

where $F(R, E)$ is the energy dependent fluence.

Where Equation 10 considers only homogeneous media, an alternative method for determining the mass range is required for application to the atmosphere. The mass

range in the atmosphere is defined to be the mass integral, $< \rho R >$, which can be written as

$$< \rho R >= \int_0^R \rho(z)\, \mathrm{d}R_B, \tag{12}$$

and is also referred to as the "areal density" [5].

2.4.5 Mass Integral Scaling

The Mass Integral Scaling (MIS) technique, based upon the mass scaling law, is well used in the study of radiation transport within the atmosphere. To better reflect the atmosphere's exponential nature, the computer codes SMAUG [1] and ATR [2] used MIS to transform flux and dose data calculated, in infinite homogeneous air, by a discrete ordinates method. Noted by Shulstad, these codes are unable to account for leakage from the top of the atmosphere, interactions between the air/ground interface, and mass distribution between source and detector [16]. The source of these deficiencies is the use of data calculated in infinite homogeneous air.

The definition of the mass range from Equation 12 delineates the mass scaling law and MIS. To illustrate how the mass scaling law is applied in variable density atmosphere, assume the medium A is the homogeneous air and that medium B is the USSA. The mass integral scaling approximation assumes that if the mass range between a source and receiver in variable density is equal to mass range in homogeneous air [5],

$$\rho_A R_A = \int_0^{R_B} \rho(z)\, \mathrm{d}R_B. \tag{13}$$

Then the $4\pi R^2$ fluence will be the same, as given by Equation 11. Transport calculations may then be calculated in a constant density atmosphere and converted to a

variable density atmosphere.

With the analytical expression for density as a function of altitude from Equation 1, an analytical expression for the mass integral, or areal density, can also be expressed as a function of altitude by

$$M_I(Z) = M_I(Z_i) + \rho(Z_i)S_i \left[1 - \exp\left(-\frac{Z - Z_i}{S_i}\right)\right], \tag{14}$$

where $M_I(Z)$ is the mass integral at a specified altitude Z, $M_I(Z_i)$ is the mass integral at the base altitude of the ith region, and S_i is the density scale height factor of the i^{th} region.

2.4.6 Effective Path Length

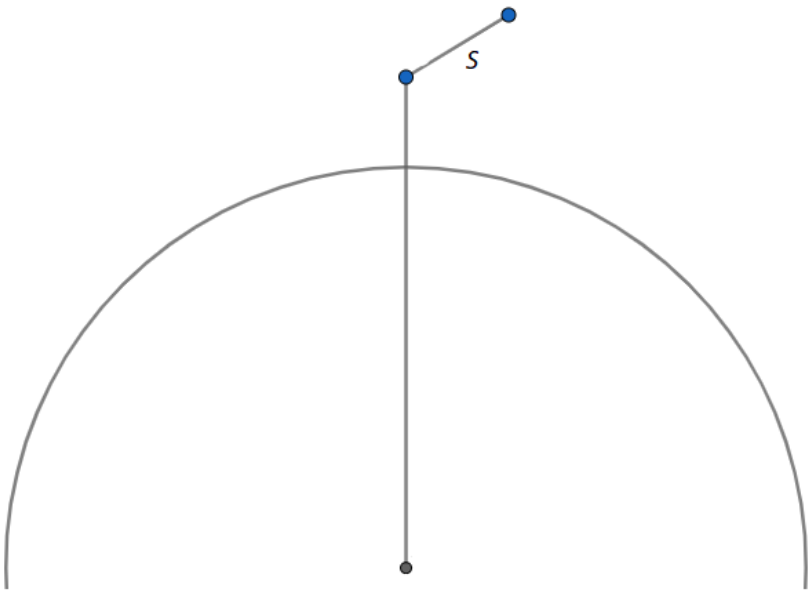

Figure 4: Example problem geometry

The effective path length (EPL), denoted as L below, describes the equivalence in

optical thickness between a path length through a medium of uniform density $\bar{\rho}$ and the actual path length through the actual medium [6]:

$$L = \int_0^{\Delta s} \frac{\rho(z_0 + \Delta z(s))}{\bar{\rho}} \, \mathrm{d}s, \tag{15}$$

where Δs is the geometric path length, z_0 is the initial geometric altitude, and $\Delta z(s)$ is the change in geometric altitude dependent upon the position, s, along the path. Considering the limitation of straight-line flight paths for neutral particles within MCNP, $\Delta z(s)$ becomes

$$\Delta z(s) = \frac{s^2 + 2r_0\zeta_0 s}{r_0^2 + \sqrt{r_0^2 + s^2 + 2r_0\zeta_0 s}}, \tag{16}$$

where r_0 is the distance from the center of the Earth at the start of the path, ζ_0 is the cosine of the zenith angle at the start of the path, and s is the length of the path (Figure 4). Relative to the MIS method, the EPL method is unique in that addresses the curvature of the Earth.

III. Methodology

3.1 Preamble

To allow for calculations in a variable density atmosphere, several alterations to the Monte Carlo N-Particle Transport Code (MCNP) source code were made to implement the Mass Integral Scaling (MIS) method. Aside from auxiliary subroutines, the main alteration involved calculating both the distance to next collision and number of mean free paths to the nearest cell boundary or detector for neutral particle. This was accomplished by adding a new subroutine named **mis**.

3.2 Assumptions

The following assumptions are made to reduce the computational complexity of the simulations:

1. The gas species in the atmosphere consists of only nitrogen and oxygen
2. The fractional composition of the gas species does not vary with altitude
3. All sources are considered point sources
4. Particles follow a straight-line path
5. The Earth is flat

3.3 Defining the Atmosphere

As mentioned in Chapter II, approximating the variation of atmospheric density with a series of continuous piece-wise exponential functions, each with a characteristic scale-height factor, allows for the mass integrals and densities at any given altitude to

be calculated analytically. In Monti's implementation of MIS, 36 regions over a range of 0 to 990 km were determined to achieve a relative error of one percent between the known density values from U.S. Standard Atmosphere, 1976 (USSA) and the exponential functions. This statement was determined to be inaccurate, as relative errors greater than one percent were found. As a result, new regions were determined such that the relative error was less than one percent. These regions are illustrated in Figure 5 alongside the the density profiles calculated with the USSA model and piece-wise approximation.

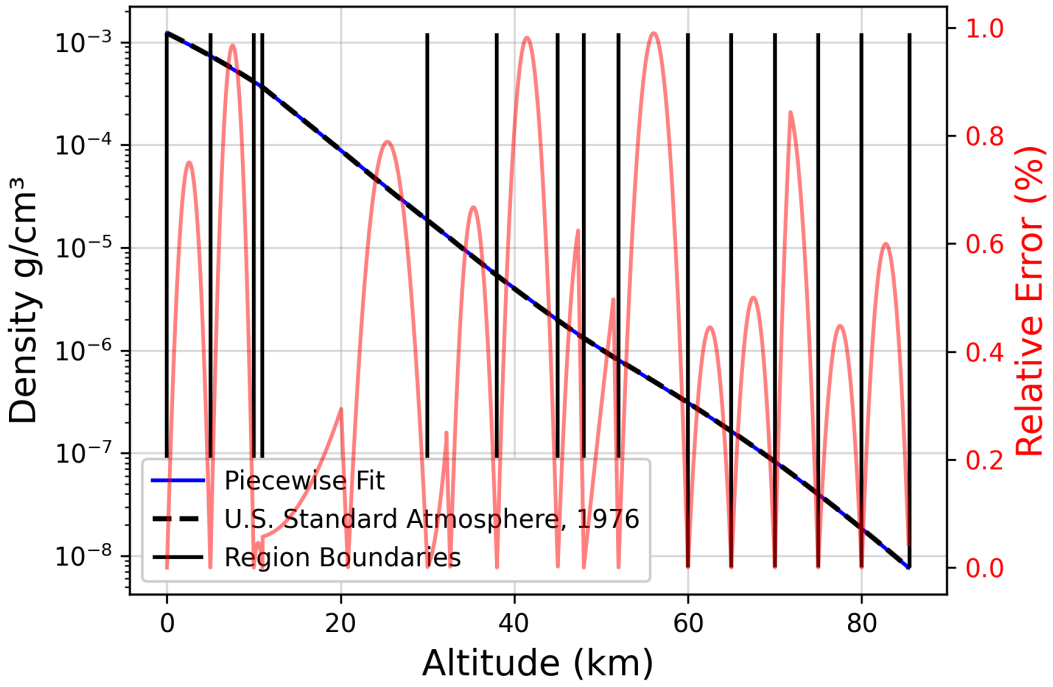

Figure 5: Density profiles and region boundaries associated with the piece-wise approximation. These regions achieve accuracy within one percent of the USSA. In addition to the improved accuracy, fewer regions were defined compared to Monti's implementation. Monti defined 16 regions below 86 km whereas there are only 14 regions below 86 km represented here.

Using known values from Table I of USSA and rearranging Equation 1, the scale height factors for 14 regions between 0 and 85.5 km were determined by

$$S_i = \frac{(Z_i - Z_{i+1})}{\ln\left[\rho(Z_{i+1})/\rho(Z_i)\right]} \tag{17}$$

where

Z_i = base altitude of ith region (cm)

Z_{i+1} = base altitude of next region (cm)

In Monti's implementation, separate scale height factors were calculated for density and mass integral in each altitude region. After calculating the density scale-height factors, this required Monti to integrate Equation 1 to calculate the mass integrals at the base altitude of each region. Once calculated, he then calculated new mass integral scale height factors in the same manner as Equation 17. Mashnik, in his implementation, concluded the density scale height factors can be used as the mass integral scale height factors as well. The implementation here follows that of Mashnik.

Both Monti and Mashnik defined the upper limit of the atmosphere as 990 km. In this work, the upper limit of the atmosphere is 85.5 km. There are a few reasons this limit is appropriate. One reason is the process of diffusive separation which occurs at altitudes greater than 86 km. Because of this process, the constituents of the atmosphere are no longer well-mixed and the second assumption listed in Section 3.2 no longer holds. Another reason for the limit of 85.5 km results from observation of the mass integral with altitude (Figure 6). At 990 km the mass integral is equal to 1031.89123 g/cm^2 whereas the mass integral at 85.5 km is equal to 1031.41948 g/cm^2 – a decrease of only 0.046 %. The latter value is referred to as the mass integral at infinity, M_{inf}. Alongside the new regions defined for the exponential fits, the new upper limit reduces the number table lookup values in the implementation.

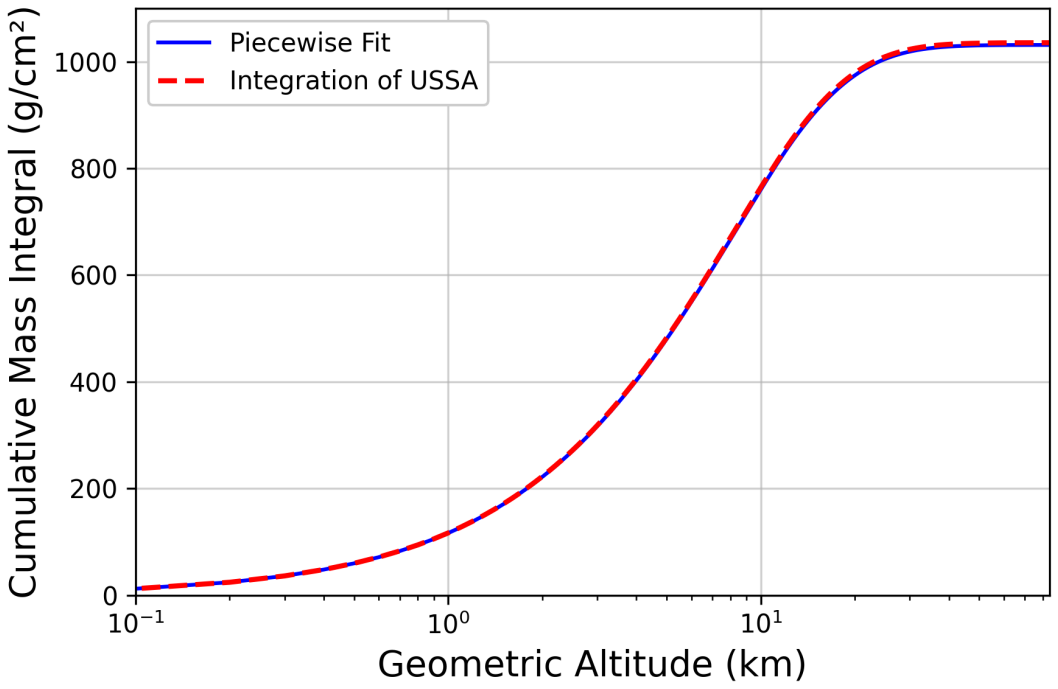

Figure 6: Profiles for the cumulative mass integral calculated by both Eq. 14 and integration of the density model provided by USSA. The integration was performed using a Clenshaw-Curtis method which uses Chebyshev moments. Relative error of the piecewise fit is within one percent of the direct integration.

3.4 Modifications to MCNP

The first modification made to the source code was to add a parameter to the MCNP cell card. Similar to indicating that a cell belongs to a universe with the U keyword, a cell may be indicated as being of variable density with the VDC (short for variable density cell) keyword. By default, VDC=0 for all cells unless indicated otherwise. When a variable density cell is indicated, the density of the cell is set to the reference density, a necessity for the MIS method, no matter the density defined by the user. The reference density used here is $1.225 \times 10^{-3} g/cm^3$ – the density of air at sea-level. The MIS method is only employed in cells indicated as variable density. Otherwise, standard MCNP calculations are performed. Additionally, the capability

for users to define their own atmosphere model with a series of altitude and density pairs was added. The user is responsible for ensuring their atmosphere model fits the exponential approximation used here for density.

To employ the MIS method, the MCNP subroutines **hstory.F90** and **transm.F90** were altered. First, the main routine for running a history of a neutral particle, subroutine **history_neutral_low** in **hstory.F90**, was altered. In this subroutine, the distance to next collision is simulated with Equation 5 relying on the microscopic cross section and atomic density of the cell the particle is located. At this point, a conditional was placed to check whether the particle is located in a variable density cell or not. If the particle is located in a variable density cell, then subroutine **mis** is called to return a new distance to collision accounting for a variable density atmosphere. As inputs, the subroutine **mis** requires the initial distance to collision (ℓ_0), the current particle altitude (Z_0), and the z-direction cosine (ω_0). Figure 7 illustrates the general system for reference.

Another call to subroutine **mis** is made when the total transmission to the detector is required. This is important when using pseudoparticles and the routine is run in **transm.F90**. The total transmission to the detector depends on the the exponential attenuation through the medium, which represents the total attenuation of the radiation by the atmosphere, along the particle path over a given number of mean free paths. Since the mean free path, which is the reciprocal of the macroscopic cross section, is initially calculated at the sea-level reference density it is necessary to correct for a variable density atmosphere. Similar to the alteration made in subroutine history_neutral_low, a conditional is placed to check whether the particle is located in a variable density cell or not. When called from **transm**, the **mis** routine requires the mean free path (λ), the distance to nearest boundary or detector (dtd), the current particle altitude (Z_0), and the z-direction cosine (ω_0).

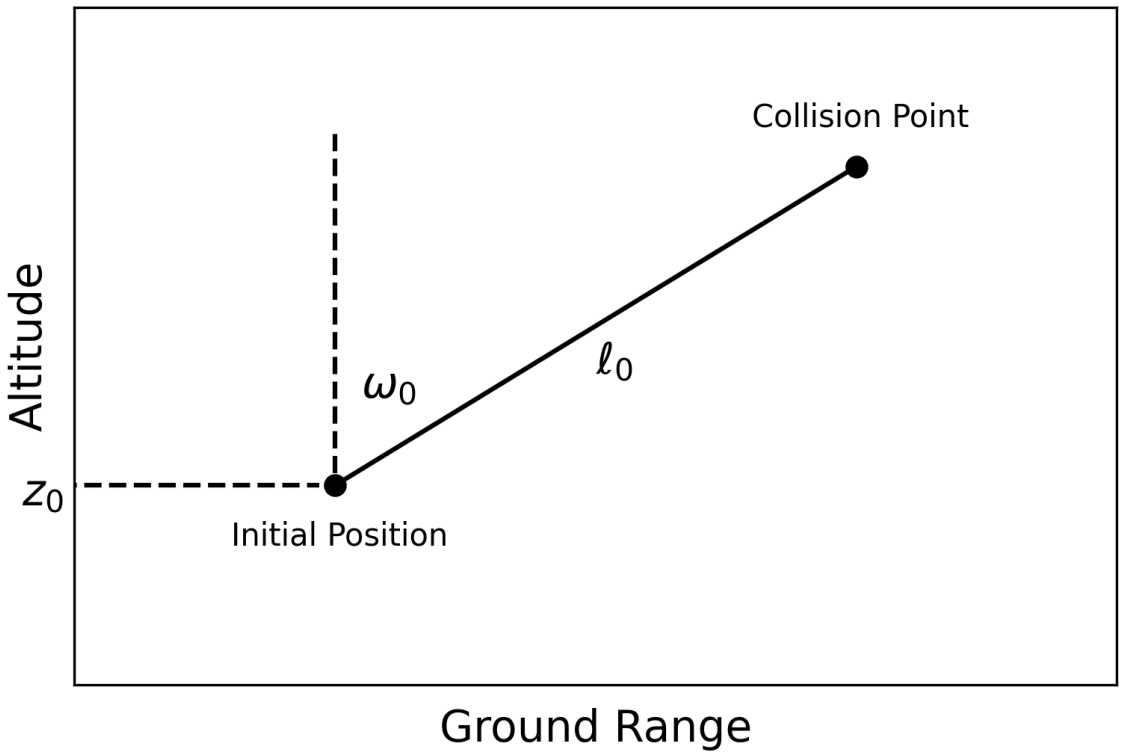

Figure 7: Reference system required by the implementation of MIS required for successful simulations of atmospheric transport.

3.5 Subroutine mis

This subroutine contains pre-computed lookup table values for the mass integrals, densities, and scale height factors of 36 regions between 0 and 88.5 km. These values can be found in Appendix A. Upon entry, the first calculation performed in subroutine **mis** is a binary search to determine which altitude region the particle is located such that $Z_i \leq Z_0 \leq Z_{i+1}$. Because the MIS technique calculates distances based on mass range, it is necessary to convert the input distance to collision to an equivalent mass range. The mass range along the particle path, ℓ_0, in a homogeneous sea-level atmosphere is calculated by

$$M_{HD} = \rho_0 \ell_0 \tag{18}$$

where

M_{HD} = equivalent mass range (g/cm^2)

ρ_0 = reference density (g/cm^3)

ℓ_0 = original distance to collision (cm)

With the index i found in the binary search, the cumulative mass integral at the current particle altitude is determined with

$$M_{CA} = M(Z_i) + \rho(Z_i) S_i \left[1 - \texttt{exp} \left(- \frac{Z_0 - Z_i}{S_i} \right) \right] \tag{19}$$

where

M_{CA} = mass integral at current particle altitude (g/cm^2)

$M(Z_i)$ = mass integral at base altitude of ith region (g/cm^2)

$\rho(Z_i)$ = density at base altitude of ith region (g/cm^3)

Z_0 = current particle altitude (cm)

Z_i = base altitude of ith region (cm)

S_i = density scale height factor of ith region (cm)

Now that the values of M_{CA}, M_{HD}, and z-direction cosine, ω_0, are known, the required cumulative mass integral at the collision altitude can be determined by

$$M_{CP} = M_{CA} + M_{HD} \cdot \omega_0 \tag{20}$$

where

M_{CA} = mass integral at current particle altitude (g/cm^2)

M_{HD} = equivalent mass range (g/cm^2)

ω_0 = zenith cosine

After the M_{CP} is found, a conditional compares the value of M_{CP} and the mass integral at infinity, M_{INF}. If M_{CP} is greater than the M_{INF}, then the subroutine **mis** is exited and returns a value of $huge\_float$ a number used to effectively eliminate any future collisions along the current particle track. Otherwise, the collision altitude Z_c is calculated by rearranging Eq. 19,

$$Z_c = Z_i + S_i \texttt{ln}\left[1 + \frac{M(Z_i) - M(Z_c)}{\rho(Z_i) S_i}\right] \tag{21}$$

Finally, the new distance to collision, ℓ, accounting for a variable density atmosphere is calculated with Eq. 22 when ω_0 is not small. In the case where ω_0 is small, the initial particle altitude and collision altitude are nearly co-altitude and the change in density along the particle path small. ω_0 is considered small whenever the difference between source and collision altitude is less than 10 meters. When this occurs, the average density between the two points is used and the distance to collision is calculated with Eq. 23

$$\ell = \frac{(Z_c - Z_0)}{\omega_0} \tag{22}$$

$$\ell = \frac{M_{HD}}{\left[\rho(Z_c) + \rho(Z_i)\right]/2} \tag{23}$$

where

$\rho(Z_c)$ = the density at the particle collision altitude (g/cm^3)

$\rho(Z_i)$ = the density at the initial particle altitude (g/cm^3)

When the **mis** subroutine is called from **transm**, a similar sequence of calculations

occurs. First it is necessary to determine the altitude of the nearest detector or boundary. This is accomplished by the following equation

$$Z_d = Z_0 + DTD \cdot \omega_0 \tag{24}$$

where

Z_d = altitude of detector or boundary (cm)

Z_0 = current particle altitude (cm)

DTD = distance to detector or boundary (cm)

ω_0 = Z-direction cosine

The mass integral along the particle path in a homogeneous atmosphere, M_{HD}, is calculated the same as before. Additionally, the cumulative mass integral at both the current particle altitude and detector altitude are calculated using Equation 19. The mass integral along the particle path in a variable density atmosphere is determined by

$$M_{PD} = \frac{M_{DA} - M_{CA}}{\omega_0} \tag{25}$$

Similar to before, where ω_0 is small, the initial particle altitude and collision altitude are nearly co-altitude and the change in density along the particle path small. ω_0 is considered small whenever the difference between source and collision altitude is less than 10 meters. When this occurs, the average density between the two points is used and the mass integral along the particle path in a variable density atmosphere is calculated with Equation 27.

$$M_{PD} = DTD \cdot \frac{\rho\left(Z_0\right) - \rho\left(Z_d\right)}{2} \tag{26}$$

The correct mean free path to the nearest detector or boundary for a variable density atmosphere can be calculated with

$$\lambda' = \frac{\lambda \cdot M_{HD}}{M_{PD}} \tag{27}$$

where

λ' = corrected mean free path (cm)

λ = original mean free path (cm)

3.5.1 Pseudocode

The general program flow follows the pseudocode below:

Algorithm 1 Algorithm for subroutine **mis.F90**

```
1: procedure MIS(ℓ_0, dtd, z_0, ω_0, flag)
2:     binary search to determine which layer particle is located
3:     calculate mass integral at z_0
4:     if flag.eq.0 then                                  ▷ Called from hstory.F90
5:         calculate mass integral along ℓ_0 in a sea-level atmosphere
6:         calculate required mass integral at collision altitude in a variable density
             atmosphere
7:         if mass integral at z_c ≤ mass integral at infinity then
8:             calculate collision altitude, z_c
9:             if ω_0 is small then
10:                calculate densities at z_0 and z_c
11:            end if
12:            calculate new distance to collision, ℓ
13:        else
14:            ℓ = huge_float
15:        end if
16:    else                                               ▷ Called from transm.F90
17:        calculate altitude at detector or boundary crossing
18:        calculate mass integral along particle path, dtd
19:        calculate mass integral at detector/boundary altitude, z_d
20:        calculate mass integral along particle path in variable density atmosphere
21:        calculate new mean free path
22:    end if
23: end procedure
```

3.6 Test Problems

As part of the verification process, a series of test problems were required. All of these problems leverage the axial symmetry allowed by the assumption of a flat-earth. At most detector positions, this assumption allows for more efficient calculations with the use of ring detectors instead of singular point detectors. For the verification process, two variants of the same problem are simulated. One simulation is performed with the sub-stepping method and standard version of MCNP requiring many cells of constant density, and the other simulation is performed with the modified version of MCNP implementing the MIS method and requiring fewer cells than its counterpart.

3.6.1 Free-Field Co-Altitude

The first of the test problems is a co-altitude source-detector problem. This test problem was chosen in part due to its use in previous studies [4][5]. However, there were several issues with the construction of the models used in the variable density and standard MCNP simulations. The first issue was the location of the source in both models. One model has the source placed at 40.05 km and the other at 40 km. A second issue was due to placement of the ring detectors. The co-altitude detectors were placed on cell boundaries; which should be avoided where possible. The third and final issue was the geometry itself. One model covered 0 to 200 km altitude while the other covered 0 to 300 km altitude. These discrepancies have the potential to introduce uncertainty when comparing the simulation results against one another and is not good practice with the goal of verification in mind. To remedy this, new models for this problem were developed.

An isotropic point source composed of a generic thermonuclear neutron spectrum was placed at 40 km and a series of co-altitude ring detectors (F5Z tally in MCNP) were placed at separation distances ranging from 1 to 100 km. For the standard

version of MCNP, a model was constructed with many vertical cells to approximate the variation of density with altitude. On the other hand, the model developed for testing the modified version of MCNP required only a single cell. Both models include a weight window mesh to employ a variance reduction technique known as splitting/roulette.

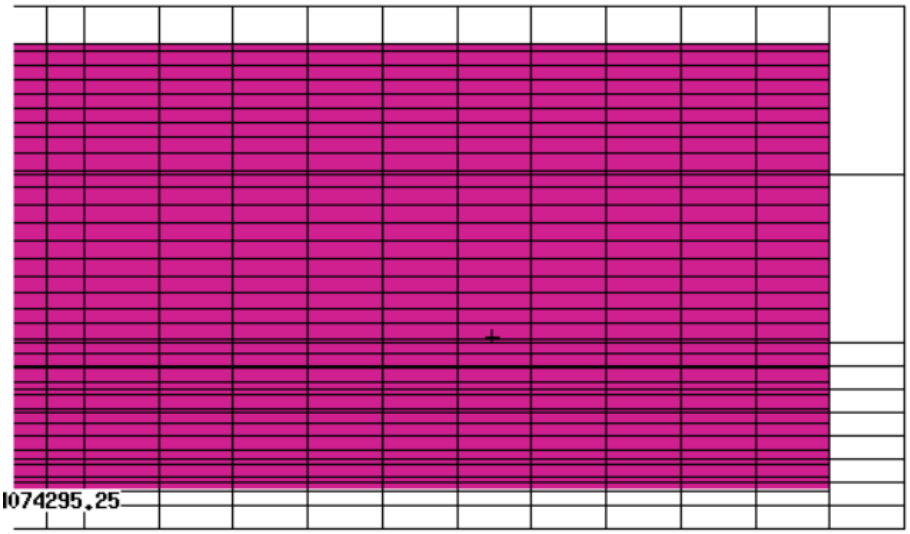

Figure 8: Model used for the standard MCNP co-altitude simulation. The mesh used for the weight window variance reduction technique is overlaid. Purple represents a multi-layered cylindrical cells.

3.6.2 Simple Free-Field

In addition to the co-altitude test problem, another test problem is simulated for verification against the standard version of MCNP. This test problem was chosen for its simplicity relative to the co-altitude test problem as it does not rely on the weight window variance reduction technique. Additionally, the generic thermonuclear neutron source spectrum was replaced with a mono-energetic 14.1 MeV source. The modified version of MCNP used a single variable density cell to estimate the neutron and secondary photon fluence at point detectors located at different source elevation

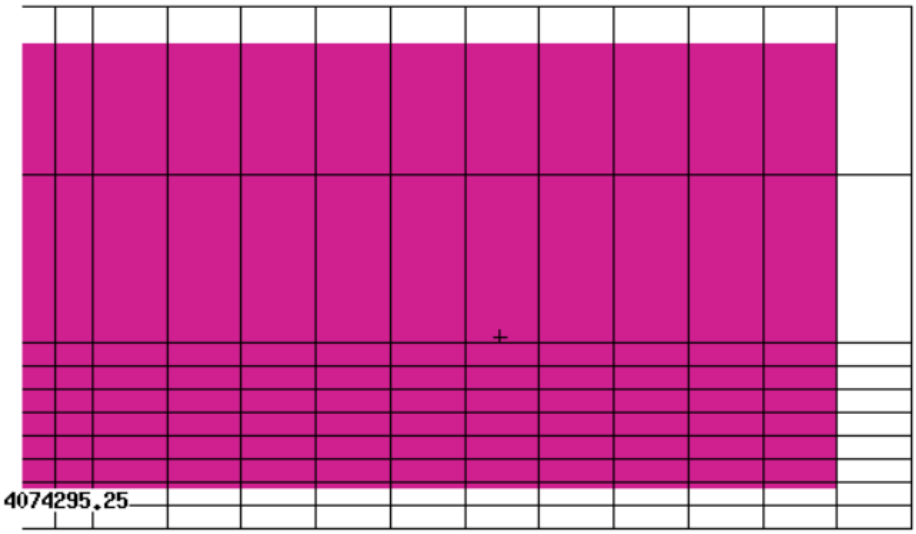

Figure 9: Model used for the variable density co-altitude simulation. The mesh used for the weight window variance reduction technique is overlaid. Purple represents a single cylindrical cell.

angles and slant ranges (Figure 10). Many simulations were run with the standard version of MCNP using the sub-stepping method.

For the sub-stepping method, an iterative approach was used to determine the vertical thickness of each layer. Layers were defined based on a specified percent change in density. For example, if a 25% change in density between each layer is desired and if 0 km is the base of the first layer, then the upper boundary of that layer is determined when the percent change between the density at 0 km and the upper boundary (or base of the next layer) becomes 25%. The density of the layer is assigned to be the density at its geometric midpoint. While assigning the density of the layer is somewhat arbitrary, it is convenient to assign the density at its geometric midpoint because the direct flux contributions from source particles to a co-altitude detector will be the same between methods[1].

[1]This is true for direct contributions made by either neutrons or photons in MODE n or MODE p problems, respectively. For MODE n p problems (with a neutron source), source photons are produced at neutron collision sites.

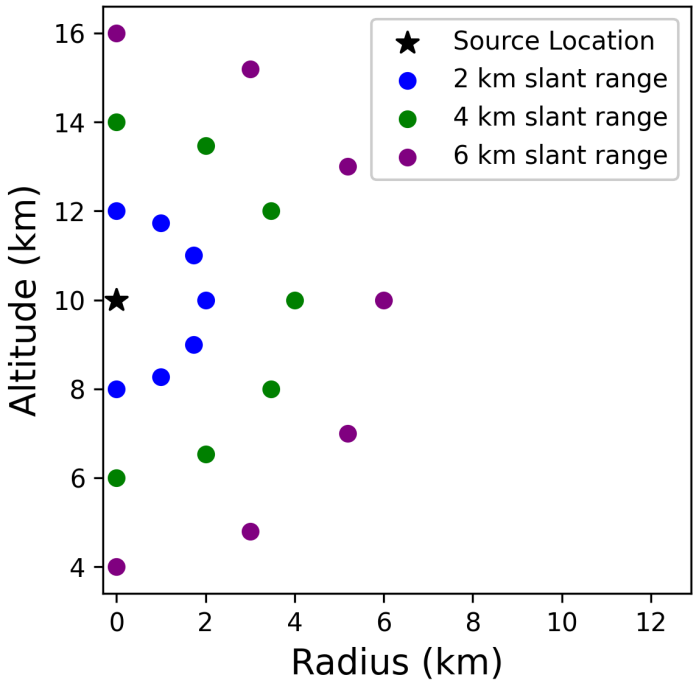

Figure 10: Detector locations associated with the simple free-field problem. A 14.1 MeV neutron source located at 10 km altitude. Detectors are placed at elevation angles of -90, -60, -30, 0, 30, 60, and 90 degrees for three different source-detector separation distances of 2, 4, and 6 km.

A caveat to this approach, however, is the incorporation of point/ring detectors in the model. As described in Section 2.3.2, the point and ring detector make use of a fictitious sphere centered about the point of interest. As a result, some layer boundaries may intersect the fictitious sphere of the detector. When reasonable, layer widths were altered to avoid the presence of different densities within the fictitious sphere which otherwise would have crossed layer boundaries.

3.6.3 Exosphere Problem

This test problem was chosen to demonstrate the function of the variable density cell indicator. For this problem, the same generic thermonuclear neutron source was placed in a void cell (a cell with zero density) at an altitude of 90 km. Aside from the

position of the source, this problem shares the same geometry as shown in Figure 9. Without the variable density cell indicator, the simulation would fault due to lost particles.

IV. Results and Analysis

4.1 Preamble

The results and analysis are presented in two main parts. The first part presents results for the free-field co-altitude problem and simple free-field problem. In this section, the integration of Mass Integral Scaling (MIS) with Monte Carlo N-Particle Transport Code (MCNP) follows only the methodology shared between Monti and Mashnik. Specifically, subroutines **hstory** and **transm** were the only physics-related subroutines of the MCNP source code to be modified. The second part presents results for both the free-field co-altitude and simple free-field problems as well as the exosphere problem. The physics-related subroutines modified to obtain these results were subroutines **hstory**, **transm**, and **tallyd**.

4.2 Part One

4.2.1 Free-Field Co-altitude Problem

The result of the revised co-altitude test problem for neutron fluence is shown in Figure 11. A small 1.12x improvement in computer time is noted for the MIS method, however, this improvement is considerably less than the 4.4x improvement inferred from Mashnik's results referenced in Chapter I. This disparity in computer time improvement suggests the model used by Mashnik for the standard MCNP simulation was over-engineered. Specifically, the geometry splitting variance reduction technique used in the previous model was inefficient. For detectors close to the source, within 10 km separation distance, the values between the two methods agree within 2% of each other. Beyond 10 km, the MIS implementation is observed to underestimate the flux in comparison to the sub-stepping method with the standard version of MCNP; with the largest percent difference of -14% observed at the furthest detector location.

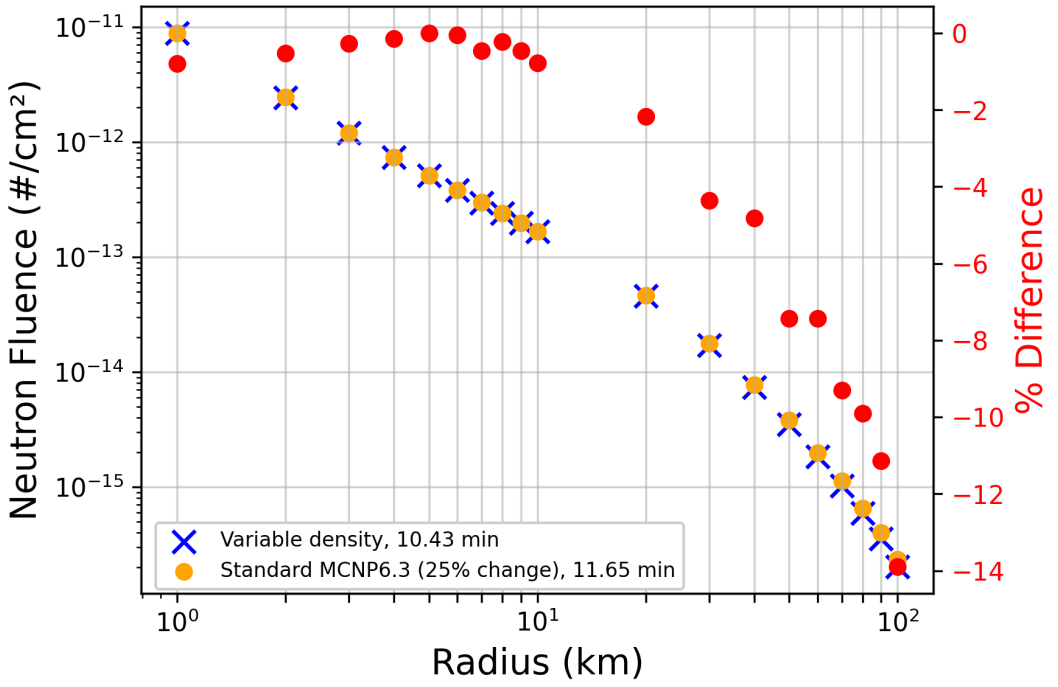

Figure 11: The standard MCNP model follows the procedure described in Sec. 3.6.2 with each layer representing a 25% decrease in density. Both models share the same weight window mesh and all tally estimates have less than 1% relative error.

4.2.2 Simple Free-Field Problem

Prior to examining the performance of the MIS modification with the standard version of MCNP, simulations with the standard version were run with different percent changes in density between layers (Figure 12). As a result, the model with a 1% change between layers was chosen to best approximate the variation in density. Specifically, this model was better able to estimate the neutron fluence for the detector at the 90 degree location. The neutron fluence for the detectors located 4 km away from the source is shown in Figure 13. A 1.7x improvement in computer time is reported between the two simulations. This improvement is greater than the improvement reported in the previous co-altitude free-field example. This is expected as there are more layers present in simple free-field example, which increase the number

of calculations performed at cell boundaries. Similar to the analysis of the co-altitude free-field problem, the MIS underestimates the fluence reported by the standard version of MCNP. The trend observed in Figure 13 is considerably more pronounced than the previous example, exhibiting percent differences between -20% and -70%. This trend suggests the methodology outlined by both Monti and Mashnik is incomplete.

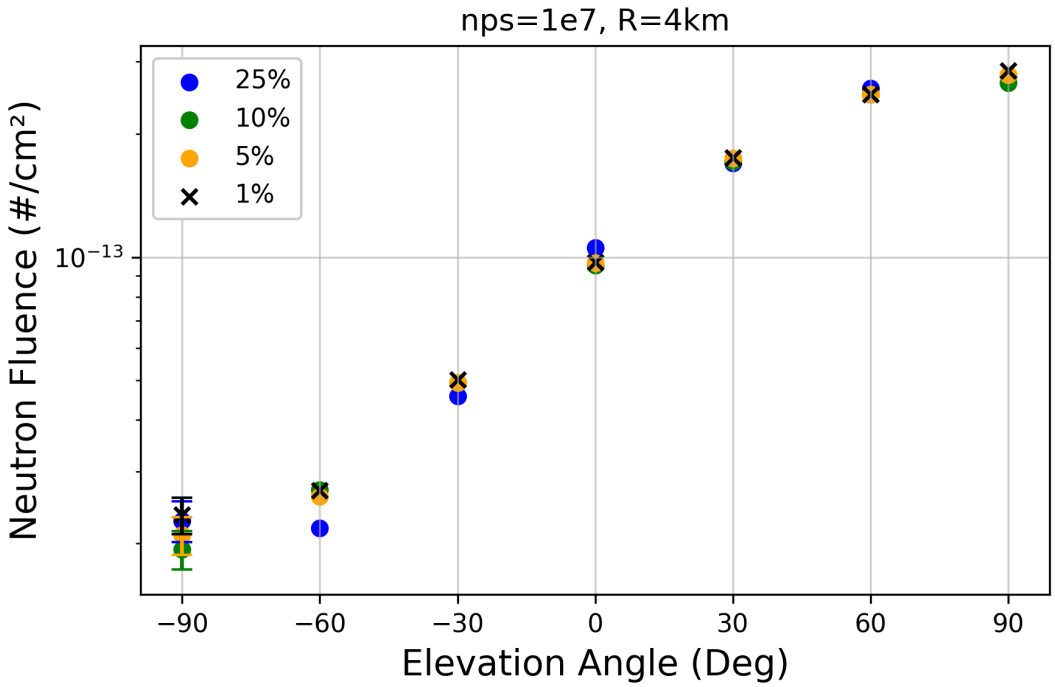

Figure 12: The MCNP models used follow the procedure described in Sec. 3.6.2 with layers representing a 25%, 10%, 5%, and 1% decrease in density. Error bars are present for tally estimates with relative errors greater than 1%. Both the 5% and 1% models show good agreement with each other with exception to the estimate at -90 degrees. Here the estimate for the latter model is noticeably larger.

Recall the discussion of the point and ring detector from Section 2.3.2. A particle's contribution to the detector is reliant on the direct transmission of a pseudoparticle from either a collision or source point. Calculation of the transmission requires knowledge of the optical thickness observed by the pseudoparticle which is calculated in the **transm** subroutine. Since the F5 tally can distinguish between total and direct

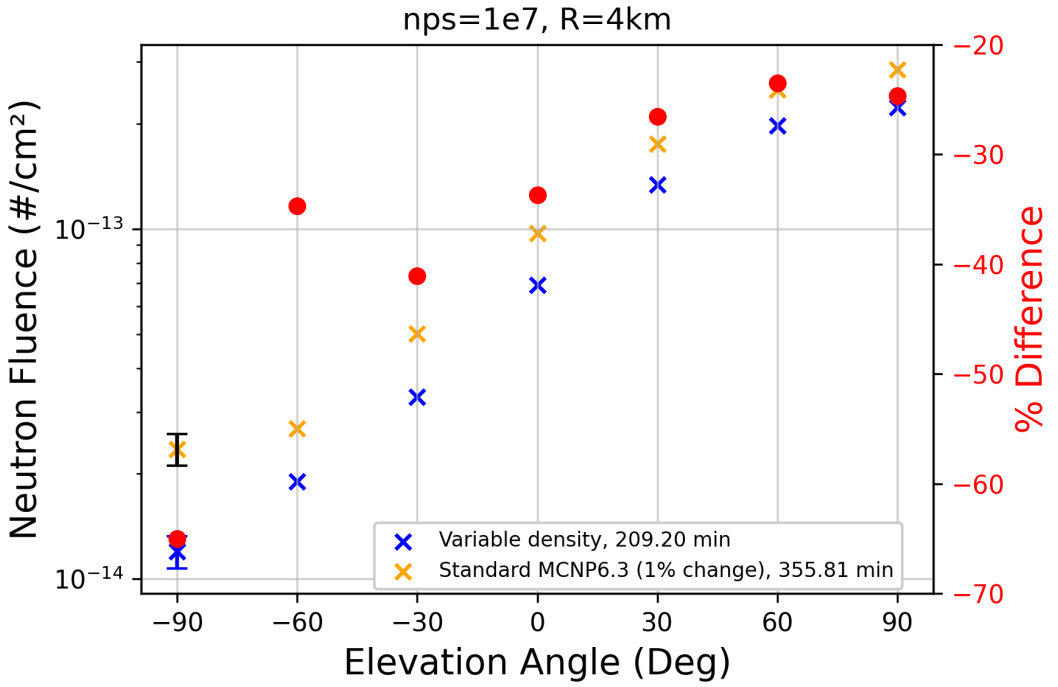

Figure 13: The standard MCNP model follows the procedure described in Sec. 3.6.2 with each layer representing a 1% decrease in density. Error bars are present for tally estimates with relative errors greater than 1%.

contributions to the detector[1], the function of the modified **transm** subroutine can be verified. The direct detector contributions separated from the total fluence reported in Figure 13 are shown in Figure 14 and exhibit great agreement between the two simulations. Therefore, the modification to subroutine **transm** functions properly and the issue lies elsewhere in the implementation of MIS within MCNP.

[1]See Section 3.6.2

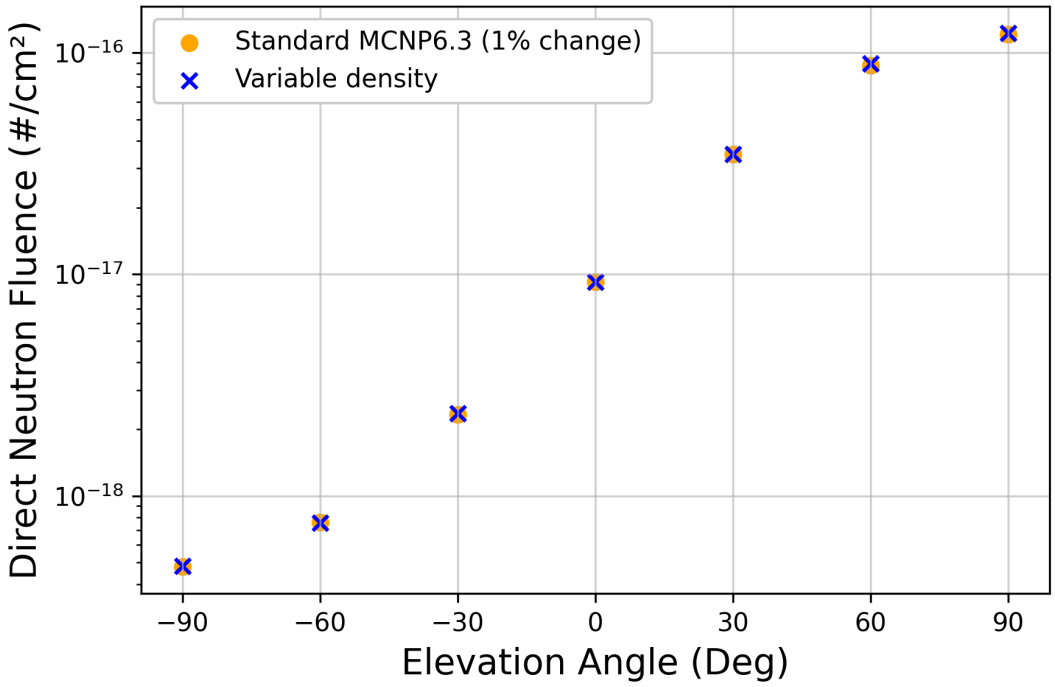

Figure 14: The standard MCNP model follows the procedure described in Sec. 3.6.2 with each layer representing a 1% decrease in density.

4.3 Part Two

In addition to the physics-related subroutines modified by Monti and Mashnik, the results presented in the following sections include the modification of subroutine **tallyd**. This subroutine is responsible for calculating contributions to the F5 tally i.e. Eq. 8 and Eq. 9 are used in this subroutine. It is speculation that previous implementations did not consider the calculation of Eq. 9 when contributions are made from particles close to the detector i.e. particles with collision points inside the fictitious sphere. When this calculation occurs in subroutine **tallyd**, a call is made to retrieve the density of the cell which the particle is currently located. This reveals an unintended side effect of initializing the density of all cells to the reference density (which is sea-level density).

Without making a correction, this leads to the macroscopic cross section being calculated with the density of sea-level instead of the actual density where the particle is located. Given the presence of the macroscopic cross section in the denominator of Eq. 9, this leads to the contribution of the particle located within the fictitious sphere to be less than if the density was calculated at the correct altitude. Therefore, it was necessary to add an additional call to subroutine **mis** which simply returns the density at the altitude of the detector.

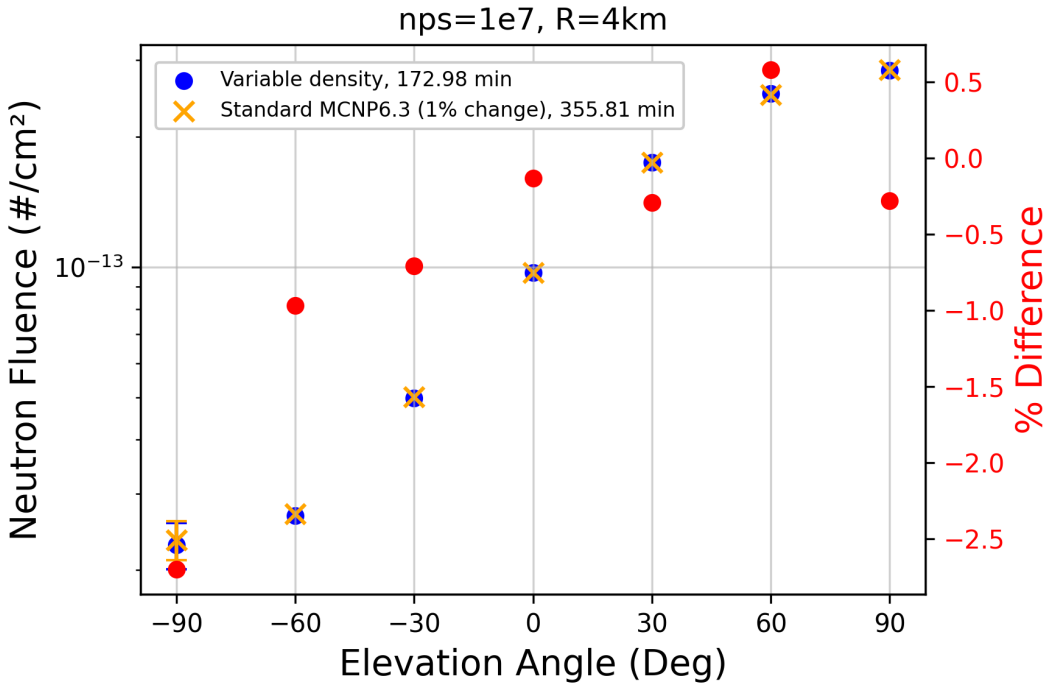

Figure 15: Neutron fluence vs elevation angle for the simple problem with a 4 km source-detector separation distance. The standard MCNP model follows the procedure described in Sec. 3.6.2 with each layer representing a 1% decrease in density. Error bars are present for tally estimates with relative errors greater than 1%.

Revisiting the simple free-field problem with the correction made to subroutine **tallyd** reveals great improvement. For the same source-detector separation distance shown in Figure 13, where observed percent differences ranged from -20% to -70%, the new results shown in Figure 15 show percent differences between -2.75% and

0.5%. Removing the outlier at -90 degrees, which both tally estimates have associated relative errors greater than 10%, the range becomes even closer – between -1% and 0.5%. It is important to note that the percent differences depicted in Figure 15 (and subsequent figures herein) are not indicative of accuracy but rather a visual indicator for agreement between the two simulations.

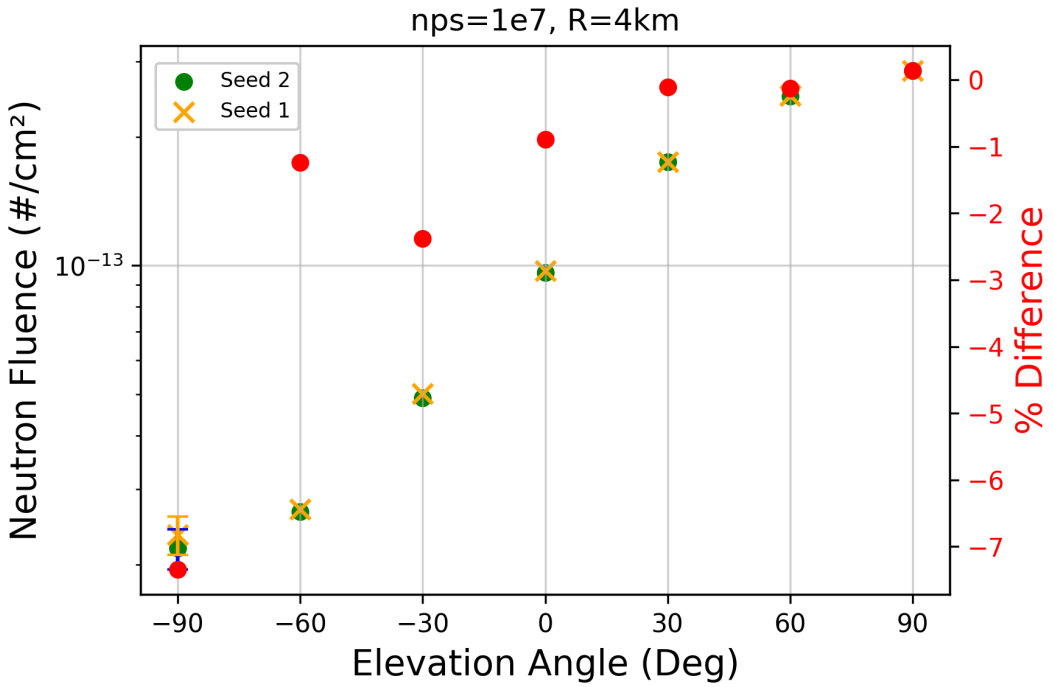

Figure 16: Comparison of neutron fluence between identical MCNP models. The only difference between the two models is the seed for the random number generator. The models follow the procedure described in Sec. 3.6.2 with each layer representing a 1% decrease in density. Error bars are present for tally estimates with relative errors greater than 1%.

In fact, the levels of precision shown are more likely a limiting factor of the Monte Carlo simulation itself. As an example, consider the results shown in Figure 16. Two identical simulations with the standard version of MCNP were run with the only difference being the seed used for the random number generator. With exception of the tally estimates at -90 degrees, a similar range of precision between the two simu-

lations is observed. Until this point, the results have focused on estimating neutron fluence but the MIS implementation works for photon fluence as well. Figures 17 and 18 compare the secondary photon fluence (photons produced from neutron interactions) between the two simulations and supports the same conclusions drawn from the neutron fluence results.

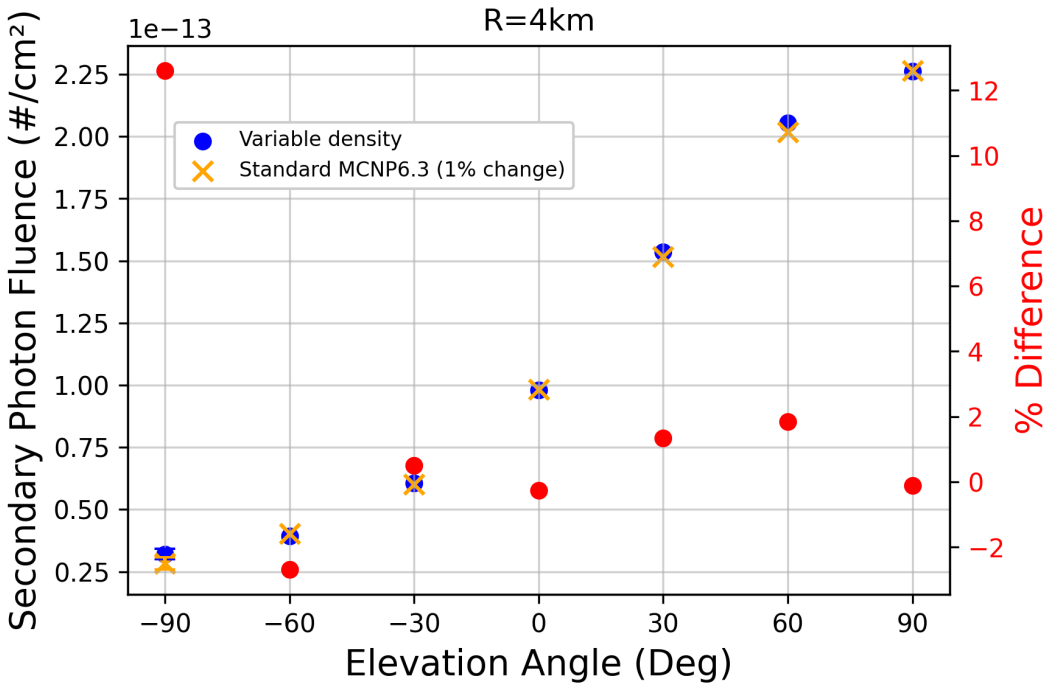

Figure 17: The standard MCNP model follows the procedure described in Sec. 3.6.2 with each layer representing a 1% decrease in density. Error bars are present for tally estimates with relative errors greater than 1%.

Additional results for the simple free-field problem can be found in Appendix B. After making the correction to subroutine **tallyd**, the co-altitude free-field problem was also revisited and significant improvements were observed. In Figure 11, percent differences up to -14% were observed. With the improved MIS the precision observed in Figure 19 between the two simulations is remarkable. While no data is shown for the exosphere problem, the simulation was able to run without losing any particles.

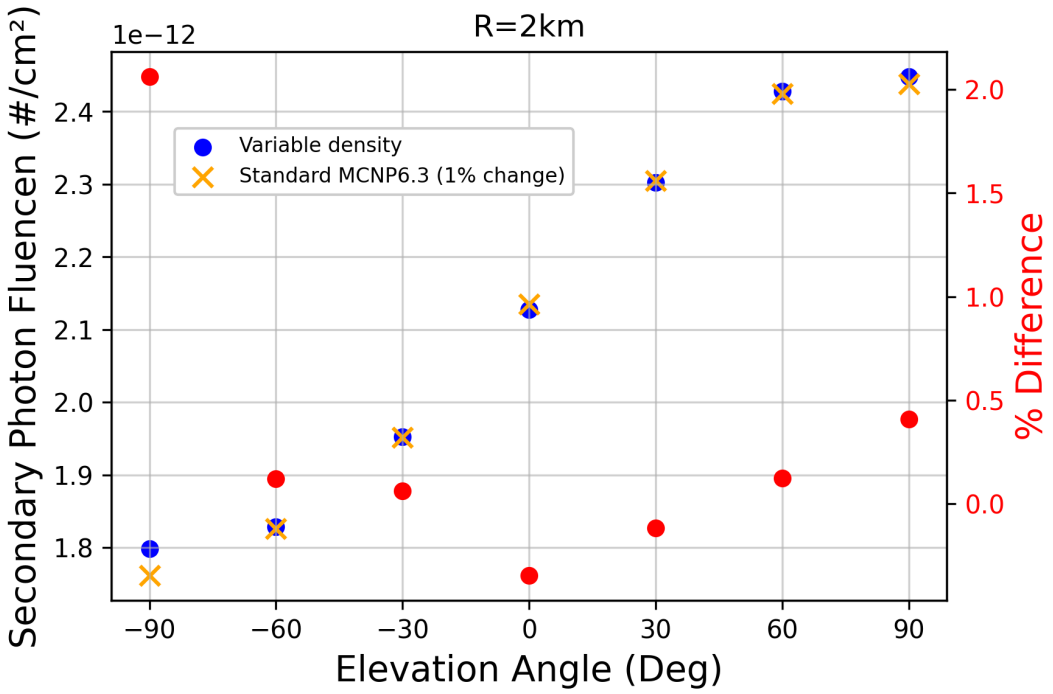

Figure 18: Secondary photon fluence vs elevation angle for the simple problem with a 2 km source-detector separation distance. The standard MCNP model follows the procedure described in Sec. 3.6.2 with each layer representing a 1% decrease in density. All tally estimates have less than 1% relative error.

However, future test problems need exploration to ensure its proper function.

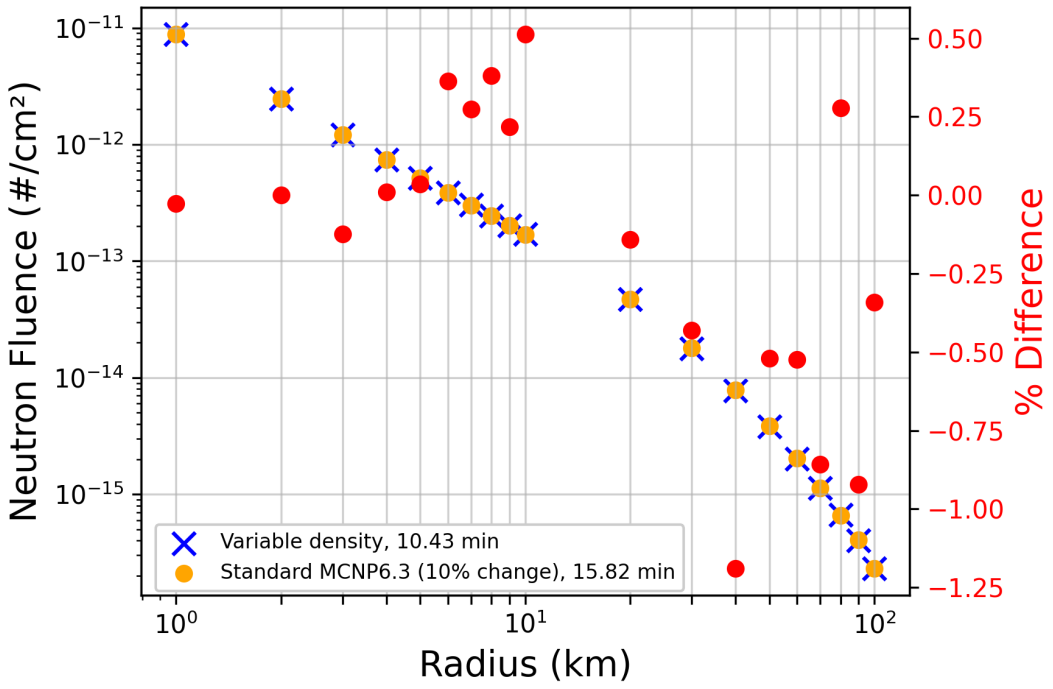

Figure 19: Neutron fluence results for co-altitude problem. The standard MCNP model follows the procedure described in Sec. 3.6.2 with each layer representing a 10% decrease in density. Both models share the same weight window mesh and all tally estimates are reported with less than 1% relative error.

V. Conclusions

The transport of radiation in the atmosphere plays a crucial role in understanding the effects of nuclear weapons. To accurately simulate the impact of prompt radiation from a nuclear explosion, it is necessary to account for the variable nature of the atmosphere. This study integrates the MIS technique with the Monte Carlo method to better simulate the transport of radiation within the atmosphere. Specifically, this work leverages and modifies the MCNP code produced by Los Alamos National Laboratory (LANL) to perform calculations based on the U.S. Standard Atmosphere, 1976 (USSA). Empirical fits to density-altitude pairs from the USSA were created to give an analytical representation of the variation of density with altitude. The analytical expression for density was extended to represent the cumulative mass integral as a function of altitude. These analytical expressions avoided the need for quadrature during transport calculations.

The modifications made to the source code for MCNP include adding a VDC keyword to indicate variable density cells, which is required to invoke the MIS method. The MIS method is only applied to variable density cells, and standard MCNP calculations are used for other cells. The **hstory.F90** and **transm.F90** subroutines were also modified to incorporate the MIS method by calling the **mis** subroutine to return a new distance to collision or mean free path, respectively, for particles located in variable density cells. The **mis** subroutine requires the initial distance to collision, the particle altitude, and the z-direction cosine as inputs.

The study examined the performance of the MIS method in comparison to the standard version of MCNP code for simulating neutron and photon fluence in atmospheric transport problems. Simulations with the standard version of MCNP were conducted by discretizing the atmosphere into constant density layers. The layers were defined based on desired percent changes in density. For the simple free-field

problem, the model with a 1% change was found to best approximate the variation in density. Initial results of the simple problem revealed improved computer time with MIS method relative to the standard version of MCNP, but it underestimated the neutron fluence. This underestimation was more pronounced than in the previous example, which was used to verify previous works, and suggests that the methodology outlined by previous works of Monti and Mashnik was incomplete.

Although initial co-altitude results comparing the standard and modified versions of MCNP agreed fairly well, it was been found that the co-altitude problem used to verify previous works may be misleading. Further investigation found the issue being related to calculation of the F5 tally when collisions occur near the detector. To remedy the issue with this calculation, a call to the **mis** subroutine was added to calculate and return the density of air at the altitude of the detector. With this improvement, great agreement between the MIS and standard MCNP was observed. In successfully implementing the MIS method, this work has provided a greater efficiency to modeling and simulation of the atmosphere with MCNP. The MCNP community can now run atmospheric transport problems without having to approximate the variation of air density – saving time by reducing model complexity and improved simulation run times.

5.1 Future Work

There are several potential areas for future work building upon the research presented here. One direction for future research could be to investigate the performance of the MIS method in simulations incorporating different media. For example, the method could be used to study the interaction between ground/air or water/air interface. Another potential area for future work is the verification of different tally types, such as cell-averaged tallies (F4 and F6), to better understand their behavior

with the MIS method. Additionally, verification work could be conducted with the High-Altitude to Space Transport Estimator (HASTE) code, which implements the effective path length (EPL) method. Finally, a user-defined option could be added to allow users to define their own altitude and density pairs, which would provide greater flexibility and applicability to a wider range of atmospheric modeling scenarios.

Appendix A. Reference Data used in Subroutine mis.F90

Region	Base Altitude (km)	Density (g/cm^3)	Mass Integral (g/cm^2)	Scale Height Factor (cm)
1	0.00	1.2250E -3	0.0	982546.1760
2	5.00	7.3643E -4	480.0423	866352.1969
3	10.00	4.1351E -4	759.8050	797878.0289
4	11.00	3.6480E -4	798.6697	636205.7465
5	30.00	1.8410E -5	1019.0450	648992.0176
6	38.00	5.3667E -6	1027.5100	697028.5403
7	45.00	1.9659E -6	1029.8804	748462.7523
8	48.00	1.3167E -6	1030.3663	814213.3677
9	52.00	8.0562E -7	1030.7825	836756.4858
10	60.00	3.0968E -7	1031.1974	780637.9400
11	65.00	1.6321E -7	1031.3118	737181.0045
12	70.00	8.2829E -8	1031.3710	647620.2009
–	85.50	7.5640E -9	1031.4195	–

Appendix B. Additional Plots for Simple Free-Field Problem

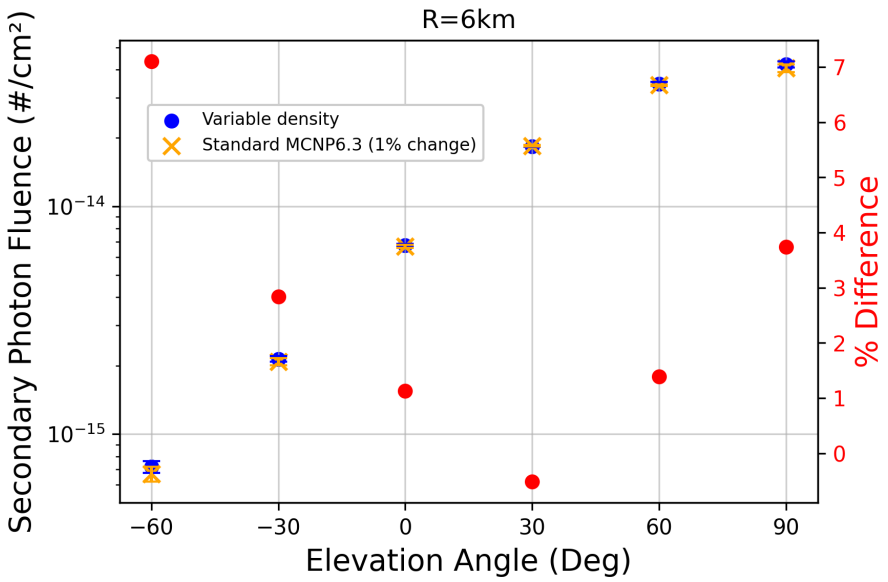

Figure 20: Secondary photon fluence vs elevation angle for the simple problem with a 6 km source-detector separation distance. The standard MCNP model follows the procedure described in Sec. 3.6.2 with each layer representing a 1% decrease in density. All tally estimates have less than 1% relative error.

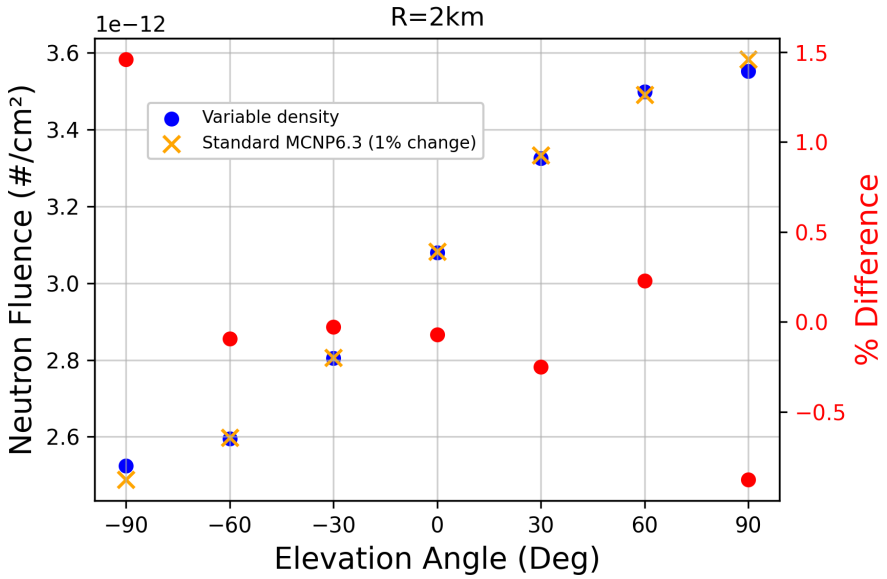

Figure 21: Neutron fluence vs elevation angle for the simple problem with a 2 km source-detector separation distance. The standard MCNP model follows the procedure described in Sec. 3.6.2 with each layer representing a 1% decrease in density. Error bars are present for tally estimates with relative errors greater than 1%.

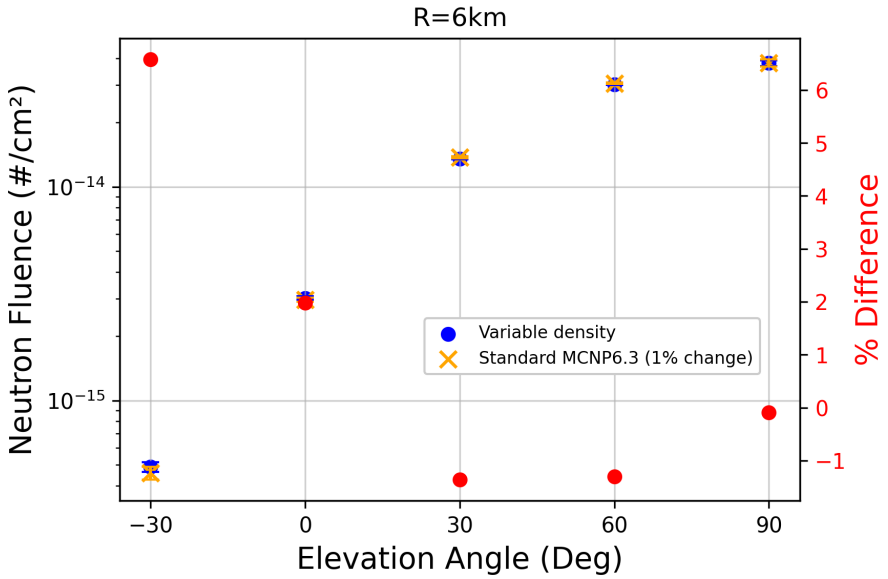

Figure 22: Neutron fluence vs elevation angle for the simple problem with a 6 km source-detector separation distance. The standard MCNP model follows the procedure described in Sec. 3.6.2 with each layer representing a 1% decrease in density. Error bars are present for tally estimates with relative errors greater than 1%.

Appendix C. MCNP Models for Free-Field Co-Altitude Problem

Example of the standard MCNP model used for the free-field co-altitude problem with layers defined by a 25% change in density.

Click  to download this file.

```
Auto Generated MCNP Deck for Layered Atmosphere
c CELL CARDS
10000  1  -7.67700E-05  2 -3 -1   imp:n=1
10100  1  -5.75710E-05  3 -4 -1   imp:n=1
10200  1  -4.31730E-05  4 -5 -1   imp:n=1
10300  1  -3.23760E-05  5 -6 -1   imp:n=1
10400  1  -2.42790E-05  6 -7 -1   imp:n=1
10500  1  -1.81890E-05  7 -8 -1   imp:n=1
10600  1  -1.36550E-05  8 -9 -1   imp:n=1
10700  1  -1.02400E-05  9 -10 -1   imp:n=1
10800  1  -7.67970E-06  10 -11 -1   imp:n=1
10900  1  -5.74300E-06  11 -12 -1   imp:n=1
11000  1  -4.31940E-06  12 -13 -1   imp:n=1
11100  1  -3.23930E-06  13 -14 -1   imp:n=1
11200  1  -2.42930E-06  14 -15 -1   imp:n=1
11300  1  -1.81800E-06  15 -16 -1   imp:n=1
11400  1  -1.36000E-06  16 -17 -1   imp:n=1
11500  1  -1.02470E-06  17 -18 -1   imp:n=1
11600  1  -7.67460E-07  18 -19 -1   imp:n=1
11700  1  -5.76290E-07  19 -20 -1   imp:n=1
11800  1  -4.32170E-07  20 -21 -1   imp:n=1
11900  1  -3.25160E-07  21 -22 -1   imp:n=1
12000  1  -2.43050E-07  22 -23 -1   imp:n=1
12100  1  -1.82450E-07  23 -24 -1   imp:n=1
12200  1  -1.36700E-07  24 -25 -1   imp:n=1
12300  1  -1.02520E-07  25 -26 -1   imp:n=1
12400  1  -7.72570E-08  26 -27 -1   imp:n=1
12500  1  -5.76580E-08  27 -28 -1   imp:n=1
12600  1  -4.32370E-08  28 -29 -1   imp:n=1
12700  1  -3.24230E-08  29 -30 -1   imp:n=1
12800  1  -2.43140E-08  30 -31 -1   imp:n=1
12900  1  -1.92960E-08  31 -32 -1   imp:n=1
99999  0  32:-2:1   imp:n=0

c SURFACE CARDS
1  cz  110.0E+05
2  pz  2.00000E+06
3  pz  2.18310E+06
4  pz  2.36620E+06
5  pz  2.54930E+06
6  pz  2.73240E+06
7  pz  2.91550E+06
8  pz  3.10010E+06
9  pz  3.28600E+06
```

```
10  pz  3.47190E+06
11  pz  3.65780E+06
12  pz  3.84740E+06
13  pz  4.04910E+06
14  pz  4.25080E+06
15  pz  4.45250E+06
16  pz  4.66460E+06
17  pz  4.88700E+06
18  pz  5.12130E+06
19  pz  5.35990E+06
20  pz  5.60070E+06
21  pz  5.84150E+06
22  pz  6.07680E+06
23  pz  6.30140E+06
24  pz  6.52460E+06
25  pz  6.73670E+06
26  pz  6.94880E+06
27  pz  7.14140E+06
28  pz  7.32780E+06
29  pz  7.51420E+06
30  pz  7.70060E+06
31  pz  7.88700E+06
32  pz  8.00000E+06

C
C DATA CARDS
C
C ISOTROPIC FISSION SOURCE AT (0,0,40.00 klicks)
SDEF  ERG=D1  POS=0 0 40.00E+5
SC1  FISSION SPECTRUM (GENERIC)
SI1  H 4.14E-7 1.1254E-6 3.059E-6 1.0677E-5 2.9023E-5 1.013E-4 5.8295E-4
         1.2341E-3 3.3546E-3 1.0333E-2 2.1875E-2 2.4788E-2 5.2475E-2
         0.1111 0.1576 0.5502 1.108 1.827 2.307 2.385
         3.012 4.066 4.724 4.966 6.376 7.408 8.187
         9.048 10.00 11.05 12.21 12.82 13.84 14.19
SP1  D 0 0 0 0 0 2.0226E-3 2.3974E-2
         4.2300E-2 7.9823E-2 1.1337E-1 8.4647E-2 1.4145E-2 8.1805E-2
         7.0979E-2 3.3869E-2 9.8584E-2 8.4961E-2 6.2051E-2 2.5916E-2 3.6882E-3
         2.2402E-2 2.6063E-2 1.2918E-2 4.0545E-3 1.8073E-2 8.6953E-3 5.8951E-3
         6.1457E-3 7.8970E-3 9.4915E-3 1.6382E-2 1.7368E-2 3.3667E-2 9.3298E-3
C
C MATERIAL SPECIFICATION
C Currently use a room temperature
M1       7014.00C -0.78
         8016.00C -0.22
C neutron flux (1/cm2) from ring detector at 40.15 km altitude
F5Z:n    40.00E5   1.00E5 0.1E5  $ n flux for R = 1 km at Z=40.15 km altitude
F15Z:n   40.00E5   2.00E5 0.1E5
F25Z:n   40.00E5   3.00E5 0.1E5
F35Z:n   40.00E5   4.00E5 0.1E5
F45Z:n   40.00E5   5.00E5 0.1E5
F55Z:n   40.00E5   6.00E5 0.1E5
F65Z:n   40.00E5   7.00E5 0.1E5
F75Z:n   40.00E5   8.00E5 0.1E5
```

```
F85Z:n   40.00E5   9.00E5 0.1E5
F95Z:n   40.00E5  10.00E5 0.1E5
F105Z:n  40.00E5  20.00E5 0.1E5
F115Z:n  40.00E5  30.00E5 0.1E5
F125Z:n  40.00E5  40.00E5 0.1E5
F135Z:n  40.00E5  50.00E5 0.1E5
F145Z:n  40.00E5  60.00E5 0.1E5
F155Z:n  40.00E5  70.00E5 0.1E5
F165Z:n  40.00E5  80.00E5 0.1E5
F175Z:n  40.00E5  90.00E5 0.1E5
F185Z:n  40.00E5 100.00E5 0.1E5
WWG  185  0  0
c MESH   REF=0 0 40.0001E5
MESH   GEOM=CYL  REF=0 0 40.0001E5  ORIGIN=0 0 15E+5
       IMESH  10E5 120E5
       IINTS  2 11
       JMESH  25E5 70E5
       JINTS  8 2
       KMESH  1
       KINTS  1
RAND GEN=2 SEED=2234895183
nps  1e6
PRINT
```

Example of the standard MCNP model used for the free-field co-altitude problem with layers defined by a 10% change in density.

Click  to download this file.

```
Auto Generated MCNP Deck for Layered Atmosphere
c CELL CARDS
10000  1  -8.40980E-05  2 -3 -1   imp:n=1
10100  1  -7.56800E-05  3 -4 -1   imp:n=1
10200  1  -6.81040E-05  4 -5 -1   imp:n=1
10300  1  -6.12870E-05  5 -6 -1   imp:n=1
10400  1  -5.51520E-05  6 -7 -1   imp:n=1
10500  1  -4.96320E-05  7 -8 -1   imp:n=1
10600  1  -4.46640E-05  8 -9 -1   imp:n=1
10700  1  -4.01930E-05  9 -10 -1   imp:n=1
10800  1  -3.61700E-05  10 -11 -1   imp:n=1
10900  1  -3.25490E-05  11 -12 -1   imp:n=1
11000  1  -2.92910E-05  12 -13 -1   imp:n=1
11100  1  -2.63590E-05  13 -14 -1   imp:n=1
11200  1  -2.37210E-05  14 -15 -1   imp:n=1
11300  1  -2.13460E-05  15 -16 -1   imp:n=1
11400  1  -1.92080E-05  16 -17 -1   imp:n=1
11500  1  -1.72870E-05  17 -18 -1   imp:n=1
11600  1  -1.55580E-05  18 -19 -1   imp:n=1
11700  1  -1.40010E-05  19 -20 -1   imp:n=1
11800  1  -1.26010E-05  20 -21 -1   imp:n=1
11900  1  -1.13400E-05  21 -22 -1   imp:n=1
12000  1  -1.02060E-05  22 -23 -1   imp:n=1
```

```
12100  1  -9.18450E-06  23 -24 -1   imp:n=1
12200  1  -8.26570E-06  24 -25 -1   imp:n=1
12300  1  -7.43870E-06  25 -26 -1   imp:n=1
12400  1  -6.69450E-06  26 -27 -1   imp:n=1
12500  1  -6.02480E-06  27 -28 -1   imp:n=1
12600  1  -5.41370E-06  28 -29 -1   imp:n=1
12700  1  -4.87970E-06  29 -30 -1   imp:n=1
12800  1  -4.39140E-06  30 -31 -1   imp:n=1
12900  1  -3.95200E-06  31 -32 -1   imp:n=1
13000  1  -3.55660E-06  32 -33 -1   imp:n=1
13100  1  -3.20070E-06  33 -34 -1   imp:n=1
13200  1  -2.88040E-06  34 -35 -1   imp:n=1
13300  1  -2.59220E-06  35 -36 -1   imp:n=1
13400  1  -2.33280E-06  36 -37 -1   imp:n=1
13500  1  -2.09940E-06  37 -38 -1   imp:n=1
13600  1  -1.88850E-06  38 -39 -1   imp:n=1
13700  1  -1.70030E-06  39 -40 -1   imp:n=1
13800  1  -1.53020E-06  40 -41 -1   imp:n=1
13900  1  -1.37660E-06  41 -42 -1   imp:n=1
14000  1  -1.23930E-06  42 -43 -1   imp:n=1
14100  1  -1.11540E-06  43 -44 -1   imp:n=1
14200  1  -1.00380E-06  44 -45 -1   imp:n=1
14300  1  -9.03430E-07  45 -46 -1   imp:n=1
14400  1  -8.12580E-07  46 -47 -1   imp:n=1
14500  1  -7.31720E-07  47 -48 -1   imp:n=1
14600  1  -6.58520E-07  48 -49 -1   imp:n=1
14700  1  -5.92640E-07  49 -50 -1   imp:n=1
14800  1  -5.33350E-07  50 -51 -1   imp:n=1
14900  1  -4.79990E-07  51 -52 -1   imp:n=1
15000  1  -4.31970E-07  52 -53 -1   imp:n=1
15100  1  -3.88750E-07  53 -54 -1   imp:n=1
15200  1  -3.49860E-07  54 -55 -1   imp:n=1
15300  1  -3.15230E-07  55 -56 -1   imp:n=1
15400  1  -2.83350E-07  56 -57 -1   imp:n=1
15500  1  -2.55000E-07  57 -58 -1   imp:n=1
15600  1  -2.29480E-07  58 -59 -1   imp:n=1
15700  1  -2.06520E-07  59 -60 -1   imp:n=1
15800  1  -1.85860E-07  60 -61 -1   imp:n=1
15900  1  -1.67390E-07  61 -62 -1   imp:n=1
16000  1  -1.50520E-07  62 -63 -1   imp:n=1
16100  1  -1.35470E-07  63 -64 -1   imp:n=1
16200  1  -1.21910E-07  64 -65 -1   imp:n=1
16300  1  -1.09720E-07  65 -66 -1   imp:n=1
16400  1  -9.87420E-08  66 -67 -1   imp:n=1
16500  1  -8.88650E-08  67 -68 -1   imp:n=1
16600  1  -8.00690E-08  68 -69 -1   imp:n=1
16700  1  -7.19650E-08  69 -70 -1   imp:n=1
16800  1  -6.47620E-08  70 -71 -1   imp:n=1
16900  1  -5.82800E-08  71 -72 -1   imp:n=1
17000  1  -5.24470E-08  72 -73 -1   imp:n=1
17100  1  -4.71970E-08  73 -74 -1   imp:n=1
17200  1  -4.24730E-08  74 -75 -1   imp:n=1
17300  1  -3.82220E-08  75 -76 -1   imp:n=1
17400  1  -3.43960E-08  76 -77 -1   imp:n=1
```

```
17500  1  -3.09530E-08  77 -78 -1   imp:n=1
17600  1  -2.78550E-08  78 -79 -1   imp:n=1
17700  1  -2.50670E-08  79 -80 -1   imp:n=1
17800  1  -2.25580E-08  80 -81 -1   imp:n=1
17900  1  -2.03000E-08  81 -82 -1   imp:n=1
18000  1  -1.84540E-08  82 -83 -1   imp:n=1
99999  0  83:-2:1   imp:n=0

c SURFACE CARDS
1  cz  110.0E5
2  pz  2.00000E+06
3  pz  2.06710E+06
4  pz  2.13420E+06
5  pz  2.20130E+06
6  pz  2.26840E+06
7  pz  2.33550E+06
8  pz  2.40260E+06
9  pz  2.46970E+06
10  pz  2.53680E+06
11  pz  2.60390E+06
12  pz  2.67100E+06
13  pz  2.73810E+06
14  pz  2.80520E+06
15  pz  2.87230E+06
16  pz  2.93940E+06
17  pz  3.00660E+06
18  pz  3.07470E+06
19  pz  3.14280E+06
20  pz  3.21090E+06
21  pz  3.27900E+06
22  pz  3.34710E+06
23  pz  3.41520E+06
24  pz  3.48330E+06
25  pz  3.55140E+06
26  pz  3.61950E+06
27  pz  3.68760E+06
28  pz  3.75570E+06
29  pz  3.82580E+06
30  pz  3.89970E+06
31  pz  3.97360E+06
32  pz  4.04750E+06
33  pz  4.12140E+06
34  pz  4.19530E+06
35  pz  4.26920E+06
36  pz  4.34310E+06
37  pz  4.41700E+06
38  pz  4.49090E+06
39  pz  4.56920E+06
40  pz  4.64810E+06
41  pz  4.72700E+06
42  pz  4.80640E+06
43  pz  4.89220E+06
44  pz  4.97800E+06
45  pz  5.06380E+06
```

```
46  pz  5.14960E+06
47  pz  5.23640E+06
48  pz  5.32460E+06
49  pz  5.41280E+06
50  pz  5.50100E+06
51  pz  5.58920E+06
52  pz  5.67740E+06
53  pz  5.76560E+06
54  pz  5.85380E+06
55  pz  5.94200E+06
56  pz  6.02820E+06
57  pz  6.11050E+06
58  pz  6.19280E+06
59  pz  6.27510E+06
60  pz  6.35740E+06
61  pz  6.43970E+06
62  pz  6.52080E+06
63  pz  6.59850E+06
64  pz  6.67620E+06
65  pz  6.75390E+06
66  pz  6.83160E+06
67  pz  6.90930E+06
68  pz  6.98700E+06
69  pz  7.05690E+06
70  pz  7.12520E+06
71  pz  7.19350E+06
72  pz  7.26180E+06
73  pz  7.33010E+06
74  pz  7.39840E+06
75  pz  7.46670E+06
76  pz  7.53500E+06
77  pz  7.60330E+06
78  pz  7.67160E+06
79  pz  7.73990E+06
80  pz  7.80820E+06
81  pz  7.87650E+06
82  pz  7.94480E+06
83  pz  8.00000E+06

C
C DATA CARDS
C
C ISOTROPIC FISSION SOURCE AT (0,0,40.00 klicks)
SDEF  ERG=D1  POS=0 0 40.00E+5
SC1  FISSION SPECTRUM (GENERIC)
SI1  H 4.14E-7 1.1254E-6 3.059E-6 1.0677E-5 2.9023E-5 1.013E-4 5.8295E-4
         1.2341E-3 3.3546E-3 1.0333E-2 2.1875E-2 2.4788E-2 5.2475E-2
         0.1111 0.1576 0.5502 1.108 1.827 2.307 2.385
         3.012 4.066 4.724 4.966 6.376 7.408 8.187
         9.048 10.00 11.05 12.21 12.82 13.84 14.19
SP1  D 0 0 0 0 0 2.0226E-3 2.3974E-2
         4.2300E-2 7.9823E-2 1.1337E-1 8.4647E-2 1.4145E-2 8.1805E-2
         7.0979E-2 3.3869E-2 9.8584E-2 8.4961E-2 6.2051E-2 2.5916E-2 3.6882E-3
         2.2402E-2 2.6063E-2 1.2918E-2 4.0545E-3 1.8073E-2 8.6953E-3 5.8951E-3
```

```
        6.1457E-3 7.8970E-3 9.4915E-3 1.6382E-2 1.7368E-2 3.3667E-2 9.3298E-3
C
C MATERIAL SPECIFICATION
C Currently use a room temperature
M1      7014.00C -0.78
        8016.00C -0.22
C neutron flux (1/cm2) from ring detector at 40.15 km altitude
F5Z:n    40.00E5   1.00E5 0.1E5  $ n flux for R = 1 km at Z=40.15 km altitude
F15Z:n   40.00E5   2.00E5 0.1E5
F25Z:n   40.00E5   3.00E5 0.1E5
F35Z:n   40.00E5   4.00E5 0.1E5
F45Z:n   40.00E5   5.00E5 0.1E5
F55Z:n   40.00E5   6.00E5 0.1E5
F65Z:n   40.00E5   7.00E5 0.1E5
F75Z:n   40.00E5   8.00E5 0.1E5
F85Z:n   40.00E5   9.00E5 0.1E5
F95Z:n   40.00E5  10.00E5 0.1E5
F105Z:n  40.00E5  20.00E5 0.1E5
F115Z:n  40.00E5  30.00E5 0.1E5
F125Z:n  40.00E5  40.00E5 0.1E5
F135Z:n  40.00E5  50.00E5 0.1E5
F145Z:n  40.00E5  60.00E5 0.1E5
F155Z:n  40.00E5  70.00E5 0.1E5
F165Z:n  40.00E5  80.00E5 0.1E5
F175Z:n  40.00E5  90.00E5 0.1E5
F185Z:n  40.00E5 100.00E5 0.1E5
WWG  185  0  0
MESH   REF=0 0 40.0001E5
C MESH   GEOM=CYL  REF=0 0 40.0001E5  ORIGIN=0 0 15E+5
C       IMESH  10E5 120E5
C      IINTS  2 11
C      JMESH  25E5 70E5
C      JINTS  8 2
C      KMESH  1
C      KINTS  1
RAND GEN=2 SEED=2234895183
nps  1e6
PRINT
```

Example of the variable density MCNP model used for the free-field co-altitude problem.

Click 📎 to download this file.

```
Single Cell model with weight windows
C Cell cards
101  1 -1.225E-3  25 -30 -1    IMP:N=1  IMP:P=1  $ Cell #101
999  0            1:-25:30     IMP:N=0     IMP:P=0       $ Outside world (void)

C Surface cards
C 23  CONCENTRIC CYLINDERS and 7 PLANES PERPENDICULAR TO Z-AXIS
1 CZ  110E+5
```

```
25 PZ  2OE+5
30 PZ  80E+5

MODE  N P
C     ISOTROPIC NEUTRON SOURCE AT (0,0,40.15 klicks)
SDEF  ERG=D1 POS=0 0 40.00E+5
SC1  SOURCE SPECTRUM (GENERIC)
SI1  H 4.14E-7 1.1254E-6 3.059E-6 1.0677E-5 2.9023E-5 1.013E-4 5.8295E-4
         1.2341E-3 3.3546E-3 1.0333E-2 2.1875E-2 2.4788E-2 5.2475E-2
         0.1111 0.1576 0.5502 1.108 1.827 2.307 2.385
         3.012 4.066 4.724 4.966 6.376 7.408 8.187
         9.048 10.00 11.05 12.21 12.82 13.84 14.19
SP1  D 0 0 0 0 0 2.0226E-3 2.3974E-2
         4.2300E-2 7.9823E-2 1.1337E-1 8.4647E-2 1.4145E-2 8.1805E-2
         7.0979E-2 3.3869E-2 9.8584E-2 8.4961E-2 6.2051E-2 2.5916E-2
         3.6882E-3 2.2402E-2 2.6063E-2 1.2918E-2 4.0545E-3 1.8073E-2
         8.6953E-3 5.8951E-3 6.1457E-3 7.8970E-3 9.4915E-3 1.6382E-2
         1.7368E-2 3.3667E-2 9.3298E-3
c
C MATERIAL SPECIFICATION
C Currently use a room temperature
M1       7014.00C -0.78
         8016.00C -0.22
C
C neutron flux (1/cm2) from ring detector
C at 40.00 km altitude
F5Z:n    40.00E5  1.00E5 0.1E5 $ n flux for R = 1 km at Z=40.00 km altitude
F15Z:n   40.00E5  2.00E5 0.1E5
F25Z:n   40.00E5  3.00E5 0.1E5
F35Z:n   40.00E5  4.00E5 0.1E5
F45Z:n   40.00E5  5.00E5 0.1E5
F55Z:n   40.00E5  6.00E5 0.1E5
F65Z:n   40.00E5  7.00E5 0.1E5
F75Z:n   40.00E5  8.00E5 0.1E5
F85Z:n   40.00E5  9.00E5 0.1E5
F95Z:n   40.00E5 10.00E5 0.1E5
F105Z:n  40.00E5 20.00E5 0.1E5
F115Z:n  40.00E5 30.00E5 0.1E5
F125Z:n  40.00E5 40.00E5 0.1E5
F135Z:n  40.00E5 50.00E5 0.1E5
F145Z:n  40.00E5 60.00E5 0.1E5
F155Z:n  40.00E5 70.00E5 0.1E5
F165Z:n  40.00E5 80.00E5 0.1E5
F175Z:n  40.00E5 90.00E5 0.1E5
F185Z:n  40.00E5 100.00E5 0.1E5
C photon  flux (1/cm2) from ring detector
C at 40.15 km altitude
c F205Z:p  40.15E5  1.00E5 0.1E5 $ photon flux for R = 1 km at Z=40.15 km altitude
c F215Z:p  40.15E5  2.00E5 0.1E5
c F225Z:p  40.15E5  3.00E5 0.1E5
c F235Z:p  40.15E5  4.00E5 0.1E5
c F245Z:p  40.15E5  5.00E5 0.1E5
c F255Z:p  40.15E5  6.00E5 0.1E5
c F265Z:p  40.15E5  7.00E5 0.1E5
```

```
c F275Z:p  40.15E5  8.00E5 0.1E5
c F285Z:p  40.15E5  9.00E5 0.1E5
c F295Z:p  40.15E5 10.00E5 0.1E5
c F305Z:p  40.15E5 20.00E5 0.1E5
c F315Z:p  40.15E5 30.00E5 0.1E5
c F325Z:p  40.15E5 40.00E5 0.1E5
c F335Z:p  40.15E5 50.00E5 0.1E5
c F345Z:p  40.15E5 60.00E5 0.1E5
c F355Z:p  40.15E5 70.00E5 0.1E5
c F365Z:p  40.15E5 80.00E5 0.1E5
c F375Z:p  40.15E5 90.00E5 0.1E5
c F385Z:p  40.15E5 100.00E5 0.1E5
C
F2:n  30 $ LEAKAGE OUT OF THE TOP SURFACE
C
C
WWG  185  0  0
MESH   REF=0 0 40.0001E5
RAND GEN=2 SEED=2234895183
NPS 1E6
c PRINT
c PRDMP j j -1
```

Appendix D. MCNP Models for Simple Free-Field Problem

Example of the standard MCNP model used for the simple problem with layers defined by a 1% change in density.

Click  to download this file.

```
Auto Generated MCNP Deck for Layered Atmosphere
c CELL CARDS
10000  1  -9.94370E-04  2 -3 -1   imp:n=1
10100  1  -9.84400E-04  3 -4 -1   imp:n=1
10200  1  -9.74530E-04  4 -5 -1   imp:n=1
10300  1  -9.64760E-04  5 -6 -1   imp:n=1
10400  1  -9.55090E-04  6 -7 -1   imp:n=1
10500  1  -9.45510E-04  7 -8 -1   imp:n=1
10600  1  -9.36030E-04  8 -9 -1   imp:n=1
10700  1  -9.26650E-04  9 -10 -1   imp:n=1
10800  1  -9.17360E-04  10 -11 -1   imp:n=1
10900  1  -9.08160E-04  11 -12 -1   imp:n=1
11000  1  -8.99060E-04  12 -13 -1   imp:n=1
11100  1  -8.90040E-04  13 -14 -1   imp:n=1
11200  1  -8.81120E-04  14 -15 -1   imp:n=1
11300  1  -8.72290E-04  15 -16 -1   imp:n=1
11400  1  -8.63540E-04  16 -17 -1   imp:n=1
11500  1  -8.54890E-04  17 -18 -1   imp:n=1
11600  1  -8.46310E-04  18 -19 -1   imp:n=1
11700  1  -8.37830E-04  19 -20 -1   imp:n=1
11800  1  -8.29430E-04  20 -21 -1   imp:n=1
11900  1  -8.21120E-04  21 -22 -1   imp:n=1
12000  1  -8.12880E-04  22 -23 -1   imp:n=1
12100  1  -8.04730E-04  23 -24 -1   imp:n=1
12200  1  -7.96670E-04  24 -25 -1   imp:n=1
12300  1  -7.88680E-04  25 -26 -1   imp:n=1
12400  1  -7.80770E-04  26 -27 -1   imp:n=1
12500  1  -7.72950E-04  27 -28 -1   imp:n=1
12600  1  -7.65200E-04  28 -29 -1   imp:n=1
12700  1  -7.57530E-04  29 -30 -1   imp:n=1
12800  1  -7.49930E-04  30 -31 -1   imp:n=1
12900  1  -7.42410E-04  31 -32 -1   imp:n=1
13000  1  -7.35110E-04  32 -33 -1   imp:n=1
13100  1  -7.27560E-04  33 -34 -1   imp:n=1
13200  1  -7.20210E-04  34 -35 -1   imp:n=1
13300  1  -7.12930E-04  35 -36 -1   imp:n=1
13400  1  -7.05720E-04  36 -37 -1   imp:n=1
13500  1  -6.98590E-04  37 -38 -1   imp:n=1
13600  1  -6.91530E-04  38 -39 -1   imp:n=1
13700  1  -6.84540E-04  39 -40 -1   imp:n=1
13800  1  -6.77620E-04  40 -41 -1   imp:n=1
13900  1  -6.70780E-04  41 -42 -1   imp:n=1
14000  1  -6.64000E-04  42 -43 -1   imp:n=1
14100  1  -6.57290E-04  43 -44 -1   imp:n=1
14200  1  -6.50640E-04  44 -45 -1   imp:n=1
```

```
14300  1  -6.44070E-04  45 -46 -1   imp:n=1
14400  1  -6.37560E-04  46 -47 -1   imp:n=1
14500  1  -6.31120E-04  47 -48 -1   imp:n=1
14600  1  -6.24740E-04  48 -49 -1   imp:n=1
14700  1  -6.18420E-04  49 -50 -1   imp:n=1
14800  1  -6.12170E-04  50 -51 -1   imp:n=1
14900  1  -6.05990E-04  51 -52 -1   imp:n=1
15000  1  -5.99860E-04  52 -53 -1   imp:n=1
15100  1  -5.93800E-04  53 -54 -1   imp:n=1
15200  1  -5.87800E-04  54 -55 -1   imp:n=1
15300  1  -5.81860E-04  55 -56 -1   imp:n=1
15400  1  -5.75980E-04  56 -57 -1   imp:n=1
15500  1  -5.70160E-04  57 -58 -1   imp:n=1
15600  1  -5.64400E-04  58 -59 -1   imp:n=1
15700  1  -5.58690E-04  59 -60 -1   imp:n=1
15800  1  -5.53050E-04  60 -61 -1   imp:n=1
15900  1  -5.47460E-04  61 -62 -1   imp:n=1
16000  1  -5.41920E-04  62 -63 -1   imp:n=1
16100  1  -5.36450E-04  63 -64 -1   imp:n=1
16200  1  -5.31030E-04  64 -65 -1   imp:n=1
16300  1  -5.25660E-04  65 -66 -1   imp:n=1
16400  1  -5.20350E-04  66 -67 -1   imp:n=1
16500  1  -5.15090E-04  67 -68 -1   imp:n=1
16600  1  -5.09880E-04  68 -69 -1   imp:n=1
16700  1  -5.04730E-04  69 -70 -1   imp:n=1
16800  1  -4.99630E-04  70 -71 -1   imp:n=1
16900  1  -4.94580E-04  71 -72 -1   imp:n=1
17000  1  -4.89580E-04  72 -73 -1   imp:n=1
17100  1  -4.84630E-04  73 -74 -1   imp:n=1
17200  1  -4.79740E-04  74 -75 -1   imp:n=1
17300  1  -4.74890E-04  75 -76 -1   imp:n=1
17400  1  -4.70090E-04  76 -77 -1   imp:n=1
17500  1  -4.65340E-04  77 -78 -1   imp:n=1
17600  1  -4.60630E-04  78 -79 -1   imp:n=1
17700  1  -4.55980E-04  79 -80 -1   imp:n=1
17800  1  -4.51370E-04  80 -81 -1   imp:n=1
17900  1  -4.46810E-04  81 -82 -1   imp:n=1
18000  1  -4.42290E-04  82 -83 -1   imp:n=1
18100  1  -4.37820E-04  83 -84 -1   imp:n=1
18200  1  -4.33400E-04  84 -85 -1   imp:n=1
18300  1  -4.29020E-04  85 -86 -1   imp:n=1
18400  1  -4.24680E-04  86 -87 -1   imp:n=1
18500  1  -4.20390E-04  87 -88 -1   imp:n=1
18600  1  -4.16140E-04  88 -89 -1   imp:n=1
18700  1  -4.11960E-04  89 -90 -1   imp:n=1
18800  1  -4.07770E-04  90 -91 -1   imp:n=1
18900  1  -4.03650E-04  91 -92 -1   imp:n=1
19000  1  -3.99580E-04  92 -93 -1   imp:n=1
19100  1  -3.95540E-04  93 -94 -1   imp:n=1
19200  1  -3.91540E-04  94 -95 -1   imp:n=1
19300  1  -3.87590E-04  95 -96 -1   imp:n=1
19400  1  -3.83670E-04  96 -97 -1   imp:n=1
19500  1  -3.79800E-04  97 -98 -1   imp:n=1
19600  1  -3.75960E-04  98 -99 -1   imp:n=1
```

```
19700  1  -3.72170E-04  99 -100 -1   imp:n=1
19800  1  -3.68410E-04  100 -101 -1   imp:n=1
19900  1  -3.64890E-04  101 -102 -1   imp:n=1
20000  1  -3.61040E-04  102 -103 -1   imp:n=1
20100  1  -3.57420E-04  103 -104 -1   imp:n=1
20200  1  -3.53840E-04  104 -105 -1   imp:n=1
20300  1  -3.50300E-04  105 -106 -1   imp:n=1
20400  1  -3.46800E-04  106 -107 -1   imp:n=1
20500  1  -3.43320E-04  107 -108 -1   imp:n=1
20600  1  -3.39890E-04  108 -109 -1   imp:n=1
20700  1  -3.36490E-04  109 -110 -1   imp:n=1
20800  1  -3.33120E-04  110 -111 -1   imp:n=1
20900  1  -3.29780E-04  111 -112 -1   imp:n=1
21000  1  -3.26480E-04  112 -113 -1   imp:n=1
21100  1  -3.23220E-04  113 -114 -1   imp:n=1
21200  1  -3.19980E-04  114 -115 -1   imp:n=1
21300  1  -3.16780E-04  115 -116 -1   imp:n=1
21400  1  -3.13610E-04  116 -117 -1   imp:n=1
21500  1  -3.10470E-04  117 -118 -1   imp:n=1
21600  1  -3.07360E-04  118 -119 -1   imp:n=1
21700  1  -3.04280E-04  119 -120 -1   imp:n=1
21800  1  -3.01240E-04  120 -121 -1   imp:n=1
21900  1  -2.98220E-04  121 -122 -1   imp:n=1
22000  1  -2.95240E-04  122 -123 -1   imp:n=1
22100  1  -2.92280E-04  123 -124 -1   imp:n=1
22200  1  -2.89360E-04  124 -125 -1   imp:n=1
22300  1  -2.86460E-04  125 -126 -1   imp:n=1
22400  1  -2.83590E-04  126 -127 -1   imp:n=1
22500  1  -2.80760E-04  127 -128 -1   imp:n=1
22600  1  -2.77950E-04  128 -129 -1   imp:n=1
22700  1  -2.75160E-04  129 -130 -1   imp:n=1
22800  1  -2.72410E-04  130 -131 -1   imp:n=1
22900  1  -2.69680E-04  131 -132 -1   imp:n=1
23000  1  -2.66980E-04  132 -133 -1   imp:n=1
23100  1  -2.64310E-04  133 -134 -1   imp:n=1
23200  1  -2.61670E-04  134 -135 -1   imp:n=1
23300  1  -2.59050E-04  135 -136 -1   imp:n=1
23400  1  -2.56450E-04  136 -137 -1   imp:n=1
23500  1  -2.53890E-04  137 -138 -1   imp:n=1
23600  1  -2.51350E-04  138 -139 -1   imp:n=1
23700  1  -2.48830E-04  139 -140 -1   imp:n=1
23800  1  -2.46340E-04  140 -141 -1   imp:n=1
23900  1  -2.43870E-04  141 -142 -1   imp:n=1
24000  1  -2.41430E-04  142 -143 -1   imp:n=1
24100  1  -2.39020E-04  143 -144 -1   imp:n=1
24200  1  -2.36620E-04  144 -145 -1   imp:n=1
24300  1  -2.34260E-04  145 -146 -1   imp:n=1
24400  1  -2.31910E-04  146 -147 -1   imp:n=1
24500  1  -2.29590E-04  147 -148 -1   imp:n=1
24600  1  -2.27290E-04  148 -149 -1   imp:n=1
24700  1  -2.25020E-04  149 -150 -1   imp:n=1
24800  1  -2.22760E-04  150 -151 -1   imp:n=1
24900  1  -2.20530E-04  151 -152 -1   imp:n=1
25000  1  -2.18330E-04  152 -153 -1   imp:n=1
```

```
25100  1  -2.16140E-04  153 -154 -1   imp:n=1
25200  1  -2.13980E-04  154 -155 -1   imp:n=1
25300  1  -2.11840E-04  155 -156 -1   imp:n=1
25400  1  -2.09720E-04  156 -157 -1   imp:n=1
25500  1  -2.07620E-04  157 -158 -1   imp:n=1
25600  1  -2.05540E-04  158 -159 -1   imp:n=1
25700  1  -2.03480E-04  159 -160 -1   imp:n=1
25800  1  -2.01440E-04  160 -161 -1   imp:n=1
25900  1  -1.99430E-04  161 -162 -1   imp:n=1
26000  1  -1.97430E-04  162 -163 -1   imp:n=1
26100  1  -1.95460E-04  163 -164 -1   imp:n=1
26200  1  -1.93500E-04  164 -165 -1   imp:n=1
26300  1  -1.91560E-04  165 -166 -1   imp:n=1
26400  1  -1.89650E-04  166 -167 -1   imp:n=1
26500  1  -1.87750E-04  167 -168 -1   imp:n=1
26600  1  -1.85870E-04  168 -169 -1   imp:n=1
26700  1  -1.84010E-04  169 -170 -1   imp:n=1
26800  1  -1.82170E-04  170 -171 -1   imp:n=1
26900  1  -1.80340E-04  171 -172 -1   imp:n=1
27000  1  -1.78540E-04  172 -173 -1   imp:n=1
27100  1  -1.76750E-04  173 -174 -1   imp:n=1
27200  1  -1.74980E-04  174 -175 -1   imp:n=1
27300  1  -1.73230E-04  175 -176 -1   imp:n=1
27400  1  -1.71500E-04  176 -177 -1   imp:n=1
27500  1  -1.69780E-04  177 -178 -1   imp:n=1
27600  1  -1.68080E-04  178 -179 -1   imp:n=1
27700  1  -1.66400E-04  179 -180 -1   imp:n=1
27800  1  -1.64730E-04  180 -181 -1   imp:n=1
27900  1  -1.63080E-04  181 -182 -1   imp:n=1
28000  1  -1.61450E-04  182 -183 -1   imp:n=1
28100  1  -1.59840E-04  183 -184 -1   imp:n=1
28200  1  -1.58240E-04  184 -185 -1   imp:n=1
28300  1  -1.56650E-04  185 -186 -1   imp:n=1
28400  1  -1.55080E-04  186 -187 -1   imp:n=1
28500  1  -1.53530E-04  187 -188 -1   imp:n=1
28600  1  -1.51990E-04  188 -189 -1   imp:n=1
28700  1  -1.50470E-04  189 -190 -1   imp:n=1
28800  1  -1.48970E-04  190 -191 -1   imp:n=1
28900  1  -1.47480E-04  191 -192 -1   imp:n=1
29000  1  -1.46000E-04  192 -193 -1   imp:n=1
29100  1  -1.44540E-04  193 -194 -1   imp:n=1
29200  1  -1.43090E-04  194 -195 -1   imp:n=1
29300  1  -1.41660E-04  195 -196 -1   imp:n=1
29400  1  -1.40240E-04  196 -197 -1   imp:n=1
29500  1  -1.38840E-04  197 -198 -1   imp:n=1
29600  1  -1.37450E-04  198 -199 -1   imp:n=1
29700  1  -1.36070E-04  199 -200 -1   imp:n=1
29800  1  -1.34710E-04  200 -201 -1   imp:n=1
29900  1  -1.33360E-04  201 -202 -1   imp:n=1
30000  1  -1.32030E-04  202 -203 -1   imp:n=1
30100  1  -1.30710E-04  203 -204 -1   imp:n=1
30200  1  -1.29400E-04  204 -205 -1   imp:n=1
30300  1  -1.28100E-04  205 -206 -1   imp:n=1
30400  1  -1.26820E-04  206 -207 -1   imp:n=1
```

```
30500  1  -1.25550E-04  207 -208 -1   imp:n=1
30600  1  -1.24290E-04  208 -209 -1   imp:n=1
30700  1  -1.23050E-04  209 -210 -1   imp:n=1
30800  1  -1.21820E-04  210 -211 -1   imp:n=1
30900  1  -1.20600E-04  211 -212 -1   imp:n=1
31000  1  -1.19390E-04  212 -213 -1   imp:n=1
31100  1  -1.18200E-04  213 -214 -1   imp:n=1
31200  1  -1.17010E-04  214 -215 -1   imp:n=1
31300  1  -1.15840E-04  215 -216 -1   imp:n=1
31400  1  -1.14680E-04  216 -217 -1   imp:n=1
31500  1  -1.13540E-04  217 -218 -1   imp:n=1
31600  1  -1.12400E-04  218 -219 -1   imp:n=1
31700  1  -1.11270E-04  219 -220 -1   imp:n=1
31800  1  -1.10160E-04  220 -221 -1   imp:n=1
31900  1  -1.09060E-04  221 -222 -1   imp:n=1
32000  1  -1.07970E-04  222 -223 -1   imp:n=1
32100  1  -1.06890E-04  223 -224 -1   imp:n=1
32200  1  -1.05820E-04  224 -225 -1   imp:n=1
32300  1  -1.04760E-04  225 -226 -1   imp:n=1
32400  1  -1.03710E-04  226 -227 -1   imp:n=1
32500  1  -1.02670E-04  227 -228 -1   imp:n=1
32600  1  -1.01640E-04  228 -229 -1   imp:n=1
32700  1  -1.00630E-04  229 -230 -1   imp:n=1
32800  1  -9.96180E-05  230 -231 -1   imp:n=1
32900  1  -9.86210E-05  231 -232 -1   imp:n=1
33000  1  -9.76340E-05  232 -233 -1   imp:n=1
33100  1  -9.66560E-05  233 -234 -1   imp:n=1
33200  1  -9.56890E-05  234 -235 -1   imp:n=1
33300  1  -9.47310E-05  235 -236 -1   imp:n=1
33400  1  -9.37830E-05  236 -237 -1   imp:n=1
33500  1  -9.28440E-05  237 -238 -1   imp:n=1
33600  1  -9.19150E-05  238 -239 -1   imp:n=1
33700  1  -9.09950E-05  239 -240 -1   imp:n=1
33800  1  -9.00840E-05  240 -241 -1   imp:n=1
33900  1  -8.91830E-05  241 -242 -1   imp:n=1
34000  1  -8.86930E-05  242 -243 -1   imp:n=1
99999  0  243:-2:1   imp:n=0

c SURFACE CARDS
1  cz  1.000000E+06
2  pz  2.00000E+05
3  pz  2.09900E+05
4  pz  2.19800E+05
5  pz  2.29700E+05
6  pz  2.39600E+05
7  pz  2.49500E+05
8  pz  2.59400E+05
9  pz  2.69300E+05
10  pz  2.79200E+05
11  pz  2.89100E+05
12  pz  2.99000E+05
13  pz  3.08900E+05
14  pz  3.18800E+05
15  pz  3.28700E+05
```

```
16  pz  3.38600E+05
17  pz  3.48500E+05
18  pz  3.58400E+05
19  pz  3.68300E+05
20  pz  3.78200E+05
21  pz  3.88100E+05
22  pz  3.98000E+05
23  pz  4.07900E+05
24  pz  4.17800E+05
25  pz  4.27700E+05
26  pz  4.37600E+05
27  pz  4.47500E+05
28  pz  4.57400E+05
29  pz  4.67300E+05
30  pz  4.77200E+05
31  pz  4.87100E+05
32  pz  4.97000E+05
33  pz  5.06100E+05
34  pz  5.14900E+05
35  pz  5.23700E+05
36  pz  5.32500E+05
37  pz  5.41300E+05
38  pz  5.50100E+05
39  pz  5.58900E+05
40  pz  5.67700E+05
41  pz  5.76500E+05
42  pz  5.85300E+05
43  pz  5.94100E+05
44  pz  6.02900E+05
45  pz  6.11700E+05
46  pz  6.20500E+05
47  pz  6.29300E+05
48  pz  6.38100E+05
49  pz  6.46900E+05
50  pz  6.55700E+05
51  pz  6.64500E+05
52  pz  6.73300E+05
53  pz  6.82100E+05
54  pz  6.90900E+05
55  pz  6.99700E+05
56  pz  7.08500E+05
57  pz  7.17300E+05
58  pz  7.26100E+05
59  pz  7.34900E+05
60  pz  7.43700E+05
61  pz  7.52500E+05
62  pz  7.61300E+05
63  pz  7.70100E+05
64  pz  7.78900E+05
65  pz  7.87700E+05
66  pz  7.96500E+05
67  pz  8.05300E+05
68  pz  8.14100E+05
69  pz  8.22900E+05
```

```
70  pz  8.31700E+05
71  pz  8.40500E+05
72  pz  8.49300E+05
73  pz  8.58100E+05
74  pz  8.66900E+05
75  pz  8.75700E+05
76  pz  8.84500E+05
77  pz  8.93300E+05
78  pz  9.02100E+05
79  pz  9.10900E+05
80  pz  9.19700E+05
81  pz  9.28500E+05
82  pz  9.37300E+05
83  pz  9.46100E+05
84  pz  9.54900E+05
85  pz  9.63700E+05
86  pz  9.72500E+05
87  pz  9.81300E+05
88  pz  9.90100E+05
89  pz  9.98900E+05
90  pz  1.00710E+06
91  pz  1.01520E+06
92  pz  1.02330E+06
93  pz  1.03140E+06
94  pz  1.03950E+06
95  pz  1.04760E+06
96  pz  1.05570E+06
97  pz  1.06380E+06
98  pz  1.07190E+06
99  pz  1.08000E+06
100  pz  1.08810E+06
101  pz  1.09620E+06
102  pz  1.10340E+06
103  pz  1.10980E+06
104  pz  1.11620E+06
105  pz  1.12260E+06
106  pz  1.12900E+06
107  pz  1.13540E+06
108  pz  1.14180E+06
109  pz  1.14820E+06
110  pz  1.15460E+06
111  pz  1.16100E+06
112  pz  1.16740E+06
113  pz  1.17380E+06
114  pz  1.18020E+06
115  pz  1.18660E+06
116  pz  1.19300E+06
117  pz  1.19940E+06
118  pz  1.20580E+06
119  pz  1.21220E+06
120  pz  1.21860E+06
121  pz  1.22500E+06
122  pz  1.23140E+06
123  pz  1.23780E+06
```

```
124  pz  1.24420E+06
125  pz  1.25060E+06
126  pz  1.25700E+06
127  pz  1.26340E+06
128  pz  1.26980E+06
129  pz  1.27620E+06
130  pz  1.28260E+06
131  pz  1.28900E+06
132  pz  1.29540E+06
133  pz  1.30180E+06
134  pz  1.30820E+06
135  pz  1.31460E+06
136  pz  1.32100E+06
137  pz  1.32740E+06
138  pz  1.33380E+06
139  pz  1.34020E+06
140  pz  1.34660E+06
141  pz  1.35300E+06
142  pz  1.35940E+06
143  pz  1.36580E+06
144  pz  1.37220E+06
145  pz  1.37860E+06
146  pz  1.38500E+06
147  pz  1.39140E+06
148  pz  1.39780E+06
149  pz  1.40420E+06
150  pz  1.41060E+06
151  pz  1.41700E+06
152  pz  1.42340E+06
153  pz  1.42980E+06
154  pz  1.43620E+06
155  pz  1.44260E+06
156  pz  1.44900E+06
157  pz  1.45540E+06
158  pz  1.46180E+06
159  pz  1.46820E+06
160  pz  1.47460E+06
161  pz  1.48100E+06
162  pz  1.48740E+06
163  pz  1.49380E+06
164  pz  1.50020E+06
165  pz  1.50660E+06
166  pz  1.51300E+06
167  pz  1.51940E+06
168  pz  1.52580E+06
169  pz  1.53220E+06
170  pz  1.53860E+06
171  pz  1.54500E+06
172  pz  1.55140E+06
173  pz  1.55780E+06
174  pz  1.56420E+06
175  pz  1.57060E+06
176  pz  1.57700E+06
177  pz  1.58340E+06
```

```
178  pz  1.58980E+06
179  pz  1.59620E+06
180  pz  1.60260E+06
181  pz  1.60900E+06
182  pz  1.61540E+06
183  pz  1.62180E+06
184  pz  1.62820E+06
185  pz  1.63460E+06
186  pz  1.64100E+06
187  pz  1.64740E+06
188  pz  1.65380E+06
189  pz  1.66020E+06
190  pz  1.66660E+06
191  pz  1.67300E+06
192  pz  1.67940E+06
193  pz  1.68580E+06
194  pz  1.69220E+06
195  pz  1.69860E+06
196  pz  1.70500E+06
197  pz  1.71140E+06
198  pz  1.71780E+06
199  pz  1.72420E+06
200  pz  1.73060E+06
201  pz  1.73700E+06
202  pz  1.74340E+06
203  pz  1.74980E+06
204  pz  1.75620E+06
205  pz  1.76260E+06
206  pz  1.76900E+06
207  pz  1.77540E+06
208  pz  1.78180E+06
209  pz  1.78820E+06
210  pz  1.79460E+06
211  pz  1.80100E+06
212  pz  1.80740E+06
213  pz  1.81380E+06
214  pz  1.82020E+06
215  pz  1.82660E+06
216  pz  1.83300E+06
217  pz  1.83940E+06
218  pz  1.84580E+06
219  pz  1.85220E+06
220  pz  1.85860E+06
221  pz  1.86500E+06
222  pz  1.87140E+06
223  pz  1.87780E+06
224  pz  1.88420E+06
225  pz  1.89060E+06
226  pz  1.89700E+06
227  pz  1.90340E+06
228  pz  1.90980E+06
229  pz  1.91620E+06
230  pz  1.92260E+06
231  pz  1.92900E+06
```

```
232  pz  1.93540E+06
233  pz  1.94180E+06
234  pz  1.94820E+06
235  pz  1.95460E+06
236  pz  1.96100E+06
237  pz  1.96740E+06
238  pz  1.97380E+06
239  pz  1.98020E+06
240  pz  1.98660E+06
241  pz  1.99300E+06
242  pz  1.99940E+06
243  pz  2.00000E+06

c DATA CARDS
MODE  n p
sdef  erg=14.1  pos=0 0 10E+5
M1    7014.00c -0.78 $ DISCRETE NITROGEN XSEC
      8016.00c -0.22 $ DISCRETE OXYGEN XSEC
C R=2km, neutrons
F105:n     0.0 0.0 8.00000E+05 0.1E5 $ zeta = -90  deg
F115Z:n   8.26795E+05  1.00000E+05 0.1E5 $ zeta = -60  deg
F125Z:n   9.00000E+05  1.73205E+05 0.1E5 $ zeta = -30  deg
F135Z:n   1.00000E+06  2.00000E+05 0.1E5 $ zeta =   0  deg
F145Z:n   1.10000E+06  1.73205E+05 0.1E5 $ zeta =  30  deg
F155Z:n   1.17321E+06  1.00000E+05 0.1E5 $ zeta =  60  deg
F165:n   0.0 0.0 1.20000E+06 0.1E5 $ zeta =  90  deg
C R=4km, neutrons
F205:n     0.0 0.0 6.00000E+05 0.1E5 $ zeta = -90  deg
F215Z:n   6.53590E+05  2.00000E+05 0.1E5 $ zeta = -60  deg
F225Z:n   8.00000E+05  3.46410E+05 0.1E5 $ zeta = -30  deg
F235Z:n   1.00000E+06  4.00000E+05 0.1E5 $ zeta =   0  deg
F245Z:n   1.20000E+06  3.46410E+05 0.1E5 $ zeta =  30  deg
F255Z:n   1.34641E+06  2.00000E+05 0.1E5 $ zeta =  60  deg
F265:n   0.0 0.0 1.40000E+06 0.1E5 $ zeta =  90  deg
C R=6km, neutrons
F305:n     0.0 0.0 4.00000E+05 0.1E5 $ zeta = -90  deg
F315Z:n   4.80385E+05  3.00000E+05 0.1E5 $ zeta = -60  deg
F325Z:n   7.00000E+05  5.19615E+05 0.1E5 $ zeta = -30  deg
F335Z:n   1.00000E+06  6.00000E+05 0.1E5 $ zeta =   0  deg
F345Z:n   1.30000E+06  5.19615E+05 0.1E5 $ zeta =  30  deg
F355Z:n   1.51962E+06  3.00000E+05 0.1E5 $ zeta =  60  deg
F365:n   0.0 0.0 1.60000E+06 0.1E5 $ zeta =  90  deg
C R=2km,  photons
F405:p     0.0 0.0 8.00000E+05 0.1E5 $ zeta = -90  deg
F415Z:p   8.26795E+05  1.00000E+05 0.1E5 $ zeta = -60  deg
F425Z:p   9.00000E+05  1.73205E+05 0.1E5 $ zeta = -30  deg
F435Z:p   1.00000E+06  2.00000E+05 0.1E5 $ zeta =   0  deg
F445Z:p   1.10000E+06  1.73205E+05 0.1E5 $ zeta =  30  deg
F455Z:p   1.17321E+06  1.00000E+05 0.1E5 $ zeta =  60  deg
F465:p   0.0 0.0 1.20000E+06 0.1E5 $ zeta =  90  deg
C R=4km,  photons
F505:p    0.0 0.0 6.00000E+05 0.1E5 $ zeta = -90  deg
F515Z:p   6.53590E+05  2.00000E+05 0.1E5 $ zeta = -60  deg
F525Z:p   8.00000E+05  3.46410E+05 0.1E5 $ zeta = -30  deg
```

```
F535Z:p   1.00000E+06  4.00000E+05 0.1E5 $ zeta =   0  deg
F545Z:p   1.20000E+06  3.46410E+05 0.1E5 $ zeta =  30  deg
F555Z:p   1.34641E+06  2.00000E+05 0.1E5 $ zeta =  60  deg
F565:p   0.0 0.0 1.40000E+06 0.1E5 $ zeta =  90  deg
C R=6km,  photons
F605:p    0.0 0.0 4.00000E+05 0.1E5 $ zeta = -90  deg
F615Z:p   4.80385E+05  3.00000E+05 0.1E5 $ zeta = -60  deg
F625Z:p   7.00000E+05  5.19615E+05 0.1E5 $ zeta = -30  deg
F635Z:p   1.00000E+06  6.00000E+05 0.1E5 $ zeta =   0  deg
F645Z:p   1.30000E+06  5.19615E+05 0.1E5 $ zeta =  30  deg
F655Z:p   1.51962E+06  3.00000E+05 0.1E5 $ zeta =  60  deg
F665:p   0.0 0.0 1.60000E+06 0.1E5 $ zeta =  90  deg
RAND GEN=2 SEED=2234895183
nps  2e7
PRINT
```

Example of the variable density MCNP model used for the simple free-field problem. Click 📎 to download this file.

```
One cell, 10km source, 2,4,6 km slant range, NPS=2e7, mode n p
C Cell cards
201  1 -1.225E-3  2 -3 -1             IMP:N=1
999  0            1:-2:3              IMP:N=0   $ Outside world (void)

C Surface cards
C 23  CONCENTRIC CYLINDERS and 7 PLANES PERPENDICULAR TO Z-AXIS
1  CZ  10.00E+5 $ Surface # 1
2  PZ  2.00E+05
3  PZ  2.00E+06

c DATA CARDS
MODE  n p
sdef  erg=14.1  pos=0 0 10E+5
M1    7014.00c -0.78 $ DISCRETE NITROGEN XSEC
      8016.00c -0.22 $ DISCRETE OXYGEN XSEC
C R=2km, neutrons
F105:n     0.0 0.0 8.00000E+05 0.1E5 $ zeta = -90  deg
F115Z:n   8.26795E+05  1.00000E+05 0.1E5 $ zeta = -60  deg
F125Z:n   9.00000E+05  1.73205E+05 0.1E5 $ zeta = -30  deg
F135Z:n   1.00000E+06  2.00000E+05 0.1E5 $ zeta =   0  deg
F145Z:n   1.10000E+06  1.73205E+05 0.1E5 $ zeta =  30  deg
F155Z:n   1.17321E+06  1.00000E+05 0.1E5 $ zeta =  60  deg
F165:n   0.0 0.0 1.20000E+06 0.1E5 $ zeta =  90  deg
C R=4km, neutrons
F205:n     0.0 0.0 6.00000E+05 0.1E5 $ zeta = -90  deg
F215Z:n   6.53590E+05  2.00000E+05 0.1E5 $ zeta = -60  deg
F225Z:n   8.00000E+05  3.46410E+05 0.1E5 $ zeta = -30  deg
F235Z:n   1.00000E+06  4.00000E+05 0.1E5 $ zeta =   0  deg
F245Z:n   1.20000E+06  3.46410E+05 0.1E5 $ zeta =  30  deg
F255Z:n   1.34641E+06  2.00000E+05 0.1E5 $ zeta =  60  deg
F265:n   0.0 0.0 1.40000E+06 0.1E5 $ zeta =  90  deg
C R=6km, neutrons
```

```
F305:n     0.0 0.0 4.00000E+05 0.1E5 $ zeta = -90  deg
F315Z:n   4.80385E+05  3.00000E+05 0.1E5 $ zeta = -60  deg
F325Z:n   7.00000E+05  5.19615E+05 0.1E5 $ zeta = -30  deg
F335Z:n   1.00000E+06  6.00000E+05 0.1E5 $ zeta =   0  deg
F345Z:n   1.30000E+06  5.19615E+05 0.1E5 $ zeta =  30  deg
F355Z:n   1.51962E+06  3.00000E+05 0.1E5 $ zeta =  60  deg
F365:n   0.0 0.0 1.60000E+06 0.1E5 $ zeta =  90  deg
C R=2km,  photons
F405:p     0.0 0.0 8.00000E+05 0.1E5 $ zeta = -90  deg
F415Z:p   8.26795E+05  1.00000E+05 0.1E5 $ zeta = -60  deg
F425Z:p   9.00000E+05  1.73205E+05 0.1E5 $ zeta = -30  deg
F435Z:p   1.00000E+06  2.00000E+05 0.1E5 $ zeta =   0  deg
F445Z:p   1.10000E+06  1.73205E+05 0.1E5 $ zeta =  30  deg
F455Z:p   1.17321E+06  1.00000E+05 0.1E5 $ zeta =  60  deg
F465:p   0.0 0.0 1.20000E+06 0.1E5 $ zeta =  90  deg
C R=4km,  photons
F505:p    0.0 0.0 6.00000E+05 0.1E5 $ zeta = -90  deg
F515Z:p   6.53590E+05  2.00000E+05 0.1E5 $ zeta = -60  deg
F525Z:p   8.00000E+05  3.46410E+05 0.1E5 $ zeta = -30  deg
F535Z:p   1.00000E+06  4.00000E+05 0.1E5 $ zeta =   0  deg
F545Z:p   1.20000E+06  3.46410E+05 0.1E5 $ zeta =  30  deg
F555Z:p   1.34641E+06  2.00000E+05 0.1E5 $ zeta =  60  deg
F565:p   0.0 0.0 1.40000E+06 0.1E5 $ zeta =  90  deg
C R=6km,  photons
F605:p    0.0 0.0 4.00000E+05 0.1E5 $ zeta = -90  deg
F615Z:p   4.80385E+05  3.00000E+05 0.1E5 $ zeta = -60  deg
F625Z:p   7.00000E+05  5.19615E+05 0.1E5 $ zeta = -30  deg
F635Z:p   1.00000E+06  6.00000E+05 0.1E5 $ zeta =   0  deg
F645Z:p   1.30000E+06  5.19615E+05 0.1E5 $ zeta =  30  deg
F655Z:p   1.51962E+06  3.00000E+05 0.1E5 $ zeta =  60  deg
F665:p   0.0 0.0 1.60000E+06 0.1E5 $ zeta =  90  deg
RAND GEN=2 SEED=2234895183
nps  2e7
PRINT
```

Appendix E. MCNP Model for Exosphere Problem

Example of the variable density MCNP model used for the exosphere problem. Click  to download this file.

```
Exosphere Problem with vdc
C Cell cards
101  1 -1.225E-3  25 -30 -1  vdc=1  IMP:N=1   $ Cell #101
201  0            30 -35 -1  vdc=0  IMP:N=1
999  0            1:-25:35   vdc=0  IMP:N=0   $ Outside world (void)

C Surface cards
C 23  CONCENTRIC CYLINDERS and 7 PLANES PERPENDICULAR TO Z-AXIS
1 CZ  110E+5
25 PZ  20E+5
30 PZ  80E+5
35 PZ  100E+5

MODE  N
C     ISOTROPIC NEUTRON SOURCE AT (0,0,40.15 klicks)
SDEF  ERG=D1 POS=0 0 90.00E+5
SC1  SOURCE SPECTRUM (GENERIC)
SI1  H 4.14E-7 1.1254E-6 3.059E-6 1.0677E-5 2.9023E-5 1.013E-4 5.8295E-4
         1.2341E-3 3.3546E-3 1.0333E-2 2.1875E-2 2.4788E-2 5.2475E-2
         0.1111 0.1576 0.5502 1.108 1.827 2.307 2.385
         3.012 4.066 4.724 4.966 6.376 7.408 8.187
         9.048 10.00 11.05 12.21 12.82 13.84 14.19
SP1  D 0 0 0 0 0 2.0226E-3 2.3974E-2
         4.2300E-2 7.9823E-2 1.1337E-1 8.4647E-2 1.4145E-2 8.1805E-2
         7.0979E-2 3.3869E-2 9.8584E-2 8.4961E-2 6.2051E-2 2.5916E-2
         3.6882E-3 2.2402E-2 2.6063E-2 1.2918E-2 4.0545E-3 1.8073E-2
         8.6953E-3 5.8951E-3 6.1457E-3 7.8970E-3 9.4915E-3 1.6382E-2
         1.7368E-2 3.3667E-2 9.3298E-3
c
C MATERIAL SPECIFICATION
C Currently use a room temperature
M1       7014.00C -0.78
         8016.00C -0.22
M2       1001.00C  2
         8016.00C  1
C
C neutron flux (1/cm2) from ring detector
C at 40.00 km altitude
F5Z:n    40.00E5  1.00E5 0.1E5 $ n flux for R = 1 km at Z=40.00 km altitude
F15Z:n   40.00E5  2.00E5 0.1E5
F25Z:n   40.00E5  3.00E5 0.1E5
F35Z:n   40.00E5  4.00E5 0.1E5
F45Z:n   40.00E5  5.00E5 0.1E5
F55Z:n   40.00E5  6.00E5 0.1E5
F65Z:n   40.00E5  7.00E5 0.1E5
F75Z:n   40.00E5  8.00E5 0.1E5
F85Z:n   40.00E5  9.00E5 0.1E5
```

```
F95Z:n   40.00E5 10.00E5 0.1E5
F105Z:n  40.00E5 20.00E5 0.1E5
F115Z:n  40.00E5 30.00E5 0.1E5
F125Z:n  40.00E5 40.00E5 0.1E5
F135Z:n  40.00E5 50.00E5 0.1E5
F145Z:n  40.00E5 60.00E5 0.1E5
F155Z:n  40.00E5 70.00E5 0.1E5
F165Z:n  40.00E5 80.00E5 0.1E5
F175Z:n  40.00E5 90.00E5 0.1E5
F185Z:n  40.00E5 100.00E5 0.1E5
WWG  185  0  0
MESH   GEOM=CYL  REF=0 0 90.0001E5  ORIGIN=0 0 15.0E+5
      IMESH  10E5 120E5
     IINTS  2 11
     JMESH  25.0E5 80.0E5
     JINTS  8 2
     KMESH  1
     KINTS  1
RAND GEN=2 SEED=2234895183
NPS 1E6
```

Bibliography

1. Murphy M. Harry. A Users Guide to the SMAUG Computer Code. Technical Report SAA-TN-71-2, Air Force Weapons Laboratory, Kirkland AFB, NM, January 1971.

2. R. J. Harris, J. A. Lonergan, and L. Huszar. Models of Radiation Transport in Air – The ATR Code. Technical Report SAI-71-557-LJ, Defense Nuclear Agency, La Jolla, CA, May 1972.

3. David L. Monti and Kirk A. Mathews. Modifications to MCNP, Version 3B: Incorporating a Variable Density Atmosphere. Technical Report AFIT/EN-TR-91-2, Air Force Institute of Technology, Wright-Patterson AFB, OH, March 1991.

4. David L. Monti. High Altitude Neutral Particle Transport Using the Monte Carlo Simulation Code MCNP with Variable Density Atmosphere. Master's thesis, Air Force Institute of Technology, Wright-Patterson AFB, OH, March 1991.

5. Stepan G. Mashnik. A Variable Density Atmosphere Model for MCNP6. Technical Report LA-UR-10-00459, Los Alamos National Laboratory, Los Alamos, NM, September 2009.

6. Whitman T. Dailey. *Special Features of the Air-to-Space Neutron Transport Problem*. PhD thesis, Air Force Institute of Technology, Wright-Patterson AFB, OH, September 2017.

7. W. Dailey, private communication, 2022.

8. *U.S. Standard Atmosphere, 1976*. National Oceanic and Atmospheric Administration, National Aeronautics and Space Administration, United States Air Force, Washington, D.C., 1976.

9. C. J. Werner (Editor). *MCNP User's Manual - Code Version 6.2*. Los Alamos National Laboratory, Los Alamos, NM, 2017.

10. X-5 Monte Carlo Team. *MCNP – A General Monte Carlo N-Particle Transport Code, Version 5*. Los Alamos National Laboratory, Los Alamos, NM, 2008.

11. Micah C. Jeroutek. Verification and Validation of Unstructured Meshing Capabilites in MCNP6. Master's thesis, Air Force Institute of Technology, Wright-Patterson AFB, OH, March 2022.

12. M.D. DeHart, R.N. Slaybaugh, J.S. Rehak, and L.M. Kerby. Weighted delta-tracking with scattering. Technical report, Idaho National Laboratory, Idaho Falls, Idaho 83415, February 2019.

13. E.R. Woodcock, T. Murphy, P.J. Hemmings, and T.C. Longworth. Techniques used in the gem code for monte carlo neutronics calculations in reactors and other systems of complex geometry. In *Proc. Conf. Applications of Computing Methods to Reactor Problems*, number ANL7050, page 557. Argonne National Laboratory, 1965.

14. L.W.G. Morgan and D. Kotlyar. Weighted-delta-tracking for monte carlo particle transport. *Annals of Nuclear Energy*, 85:1184–1188, 2015.

15. Forrest B. Brown and Martin R. William. Direct sampling of monte carlo flight paths in media with continuosly varying cross-sections. In *Proc. of Nuclear Mathematical and Computational Science*, ANS Mathematical and Computational Topical Meeting, Gatlinburg, TN, April 6-11, 2003.

16. Raymond A. Shulstad. *An Evaluation of Mass Integral Scaling as Applied to the Atmospheric Radiation Transport Problem*. PhD thesis, Air Force Institute of Technology, Wright-Patterson AFB, OH, November 1976.

17. C. D. Zerby. Radiation Flux Transformation as a Function of Density of an Infinite Medium with Anisotropic Point Sources. Technical Report ORNL-2100, Oak Ridge National Laboratory, Oak Ridge, TN, October 1965.

Acronyms

CSGs constructive solid geometries. 8

EPL effective path length. 2, 17, 18, 47

HASTE High-Altitude to Space Transport Estimator. 2, 47

LANL Los Alamos National Laboratory. 2, 8, 45

MCNP Monte Carlo N-Particle Transport Code. iv, viii, 2, 3, 8, 10, 18, 19, 22, 23, 30, 31, 32, 35, 36, 37, 38, 41, 45, 46

MIS Mass Integral Scaling. iv, 2, 3, 16, 18, 19, 20, 22, 23, 24, 30, 35, 36, 37, 38, 42, 45, 46, 47

UM unstructured mesh. 8

USSA U.S. Standard Atmosphere, 1976. 3, 4, 16, 20, 22, 45

REPORT DOCUMENTATION PAGE

Form Approved
OMB No. 0704–0188

1. REPORT DATE *(DD–MM–YYYY)*	2. REPORT TYPE	3. DATES COVERED *(From — To)*
23–03–2023	Master's Thesis	Sept 2021 — Mar 2023

4. TITLE AND SUBTITLE

A Method for Monte Carlo Neutral-Particle Radiation Transport In a Variable Density Atmosphere

5a. CONTRACT NUMBER

5b. GRANT NUMBER

5c. PROGRAM ELEMENT NUMBER

6. AUTHOR(S)

Edens, Aidan

5d. PROJECT NUMBER

5e. TASK NUMBER

5f. WORK UNIT NUMBER

7. PERFORMING ORGANIZATION NAME(S) AND ADDRESS(ES)

Air Force Institute of Technology
Graduate School of Engineering and Management (AFIT/EN)
2950 Hobson Way
WPAFB OH 45433-7765

8. PERFORMING ORGANIZATION REPORT NUMBER

AFIT-ENP-MS-23-M-082

9. SPONSORING / MONITORING AGENCY NAME(S) AND ADDRESS(ES)

National Nuclear Security Administration (NNSA)
ATTN: Susan Norwood, NA-115
1000 Independence Ave SW
Washington D.C. 20585

10. SPONSOR/MONITOR'S ACRONYM(S)

NNSA

11. SPONSOR/MONITOR'S REPORT NUMBER(S)

12. DISTRIBUTION / AVAILABILITY STATEMENT

DISTRIBUTION STATEMENT A:
APPROVED FOR PUBLIC RELEASE; DISTRIBUTION UNLIMITED.

13. SUPPLEMENTARY NOTES

14. ABSTRACT

This study focuses on accurately simulating the transport of radiation in the atmosphere to better understand the effects of nuclear weapons. The variable nature of the atmosphere poses a challenge in accurately simulating the prompt radiation following a nuclear explosion. To address this challenge, the Mass Integral Scaling technique is integrated with the Monte Carlo method to perform calculations in a variable density atmosphere. In addition to previous free-field estimates, this work also enables the simulation of transport calculations with other media, such as clouds. Results of neutron and photon fluence have been verified against the standard version of MCNP and improvements in simulation run times and model complexity have been observed.

15. SUBJECT TERMS

Monte Carlo (MC), Monte Carlo N-Particle Transport code (MCNP), atmospheric radiation transport, radiation transport, Mass Integral Scaling (MIS), variable density atmosphere

16. SECURITY CLASSIFICATION OF:			17. LIMITATION OF ABSTRACT	18. NUMBER OF PAGES	19a. NAME OF RESPONSIBLE PERSON
a. REPORT	b. ABSTRACT	c. THIS PAGE			Dr. Whitman Dailey, AFIT/ENG
U	U	U	UU	90	19b. TELEPHONE NUMBER *(include area code)* (937) 255-3636 x4586; whitman.dailey@afit.edu